ON THE ADDED MASS OF A SPHERE IN A CIRCULAR CYLINDER CONSIDERING REAL FLUID EFFECTS

Thesis by

Stanley Brun Mellsen

In Partial Fulfillment of the Requirements

for the Degree of

Mechanical Engineer

California Institute of Technology

Pasadena, California

1966

ABSTRACT

An experimental method combined with boundary layer theory is given for evaluating the added mass of a sphere moving along the axis of a circular cylinder filled with water or oil. The real fluid effects are separated from ideal fluid effects.

The experimental method consists essentially of a magnetic steel sphere propelled from rest by an electromagnetic coil in which the current is accurately controlled so that it only supplies force for a short time interval which is within the laminar flow regime of the fluid. The motion of the sphere as a function of time is recorded on single frame photographs using a short-arc multiple flash lamp with accurately controlled time intervals between flashes.

A concept of the effect of boundary layer displacement on the fluid flow around a sphere is introduced to evaluate the real fluid effects on the added mass. Surprisingly accurate agreement between experiment and theory is achieved.

ACKNOWLEDGMENTS

The writer wishes to express his sincere appreciation for the encouragement and generous assistance by his advisor, Professor A. T. Ellis, throughout the course of his studies.

Sincere thanks are also due to Professor A. J. Acosta who acted as his advisor while Professor Ellis was away and to Dr. J. G. Waugh for his assistance with the experimental work.

He is further grateful to Professor T. Y. Wu and Professor G. W. Housner, the members of the faculty of the California Institute of Technology who were on his committee, and to Professor W. R. Smythe for his assistance in the electromagnetic aspects of the work.

The writer appreciates the tuition scholarships and research assistanceships awarded to him throughout his graduate education by the California Institute of Technology.

He also feels deeply indebted to Carl Eastvedt, Cecilia Lin and Zora Harrison for their help with the illustrations, Phyllis Henderson for her help on the manuscript, and Carlos Sepulveda and George Lundgren and the other members of the Hydrodynamics Laboratory who helped to build and maintain the experimental apparatus.

TABLE OF CONTENTS

ON THE ADDED MASS OF A SPHERE IN A CIRCULAR CYLINDER CONSIDERING REAL FLUID EFFECTS

I. INTRODUCTION

Qualitatively the idea of added mass is a familiar one. For example, let your hand be dipped into still water and then suddenly give a rapid acceleration broadside. The resistance to acceleration of the hand is greatly increased by the water around it. The increased resistance is due to the "virtual mass" of the hand. The difference between the real mass and the virtual mass is called the "added mass".

Added mass was first given an exact mathematical interpretation by Green and Stokes in 1833 and 1843 (1). They evaluated the added mass of a sphere in rectilinear accelerating motion in an ideal fluid of infinite extent and arrived at the following classical result. The kinetic energy of the fluid is equal to that which would be possessed by a particle moving with the same speed as the sphere and whose mass m is equal to half the mass of displaced fluid. Thus a sphere in an ideal fluid is dynamically equivalent to a heavier sphere in a vacuum whose virtual mass $M' = M + m$ is the mass M of the sphere plus an "added mass" m equal to half the mass of the displaced fluid, but whose moment of inertia is unchanged.

The theoretical basis for calculating the added mass of a general nonspherical body was done by Kelvin and Kirchhoff who

applied classical Lagrangian dynamics to the problem (1), (2). They showed that the added mass is a symmetric tensor of the second rank. For motion of a spherically symmetric body along an axis of symmetry this tensor reduces to a pseudo scalar.

All the work described to this point has been for ideal fluids. The purpose of the present investigation is to study experimentally the real fluid effects on the added mass of a sphere with the aid of boundary layer theory used in conjunction with the theoretical knowledge of ideal fluids. In these experiments a sphere is accelerated from rest without rotation vertically along the axis of a circular cylinder and the motion before the onset of boundary layer separation is studied. In this region boundary layer theory can be used to evaluate viscous forces. Also the flow about the sphere is axially symmetric and in this work the added mass tensor was considered to be a simple scalar.

II. THEORETICAL EVALUATION OF ADDED MASS FOR AN IDEAL FLUID

In the paper entitled "The Flow Around a Spheroid in a Circular Tube" by W. R. Smythe (3) is defined an equivalent length ΔL. According to Smythe this equivalent length gives the electrical resistance increase of a solid conducting cylinder due to the presence of a coaxial non-conducting spheroid inside it in terms of the equivalent cylinder length. The specific formula for a sphere in a circular cylinder is given as

$$\Delta L = \frac{4R_o^3 C_o}{3a^2} \qquad \text{(Eq. 1)}$$

where

R_o is the radius of the sphere

a is the radius of the cylinder

C_o is a function of the ratio $\frac{R_o}{a}$.

The equivalent length ΔL can also be used analogously in ideal fluid flow to determine the added mass of a sphere accelerated along the axis of an infinitely long circular cylinder. In this physical situation the length ΔL is the increase in resistance to acceleration of the flow in a cylinder filled with fluid due to the presence of a coaxial immovable sphere inside it in terms of the mass of fluid in the equivalent cylinder length. Alternatively, if the

bulk of the fluid remains at rest, the length ΔL is the increase in resistance to acceleration of the sphere in terms of the mass of fluid in the circular cylinder of length ΔL. Included in the equivalent cylinder length is the mass of fluid displaced by the sphere itself which does not contribute to the fluid inertia.

Thus

$$\rho A \Delta L = m + \rho V \qquad \text{(Eq. 2)}$$

where

A is the cross sectional area of the cylinder

ρ is the density of the fluid

m is the added mass of the sphere in the fluid

V is the volume displaced by the sphere.

Then using Eq. 1 the L.H.S. of Eq. 2 can be written

$$\rho A \Delta L = \rho(\pi a^2)\left(\frac{4R_o^3 C_o}{3a^2}\right) = \frac{4}{3}\pi R_o^3 \rho C_o = \rho V C_o$$

Thus Eq. 2 reduces to the following simple relationship between the constant C_o and the added mass coefficient:

$$\frac{m}{\rho V} = C_o - 1 \qquad \text{(Eq. 3)}$$

The values of C_o for various ratios $\frac{R_o}{a}$ are tabulated to eight significant figures in Smythe's paper (3). The following table of added mass coefficients for various ratios of sphere radius to cylinder radius is derived from the paper.

TABLE I

Added Mass Coefficient For Various Sphere to Cylinder Ratios

Radius Ratio $\frac{R_o}{a}$	Added Mass Coefficient $\frac{m}{\rho V}$
0.1	0.5012
0.2	0.5096
0.3	0.5330
0.4	0.5806
0.5	0.6660
0.6	0.8127
0.7	1.0693
0.8	1.5653
0.9	2.8351
0.95	4.7915

III. EXPERIMENTAL EVALUATION OF ADDED MASS APPROXIMATING IDEAL FLUID CONDITIONS

A. Basic Principles Used

It is theoretically possible to evaluate the added mass of a sphere in a cylinder by applying an electromagnetic impulse to a steel sphere in a vacuum and applying an identical impulse to a sphere in a dense fluid of negligible viscosity and comparing the velocities obtained at the end of the propulsive force pulse.

For the sphere launched from rest in an ideal fluid vertically upward in the earth's gravitational field, equating the total impulse applied to the sphere to its corresponding momentum change gives

$$I_w = \int_0^{T/2} (F_w - G_w)\, dt = (M + m)U_w \qquad \text{(Eq. 4)}$$

where

F_w is the electromagnetic propulsive force

G_w is the negative buoyancy force on the sphere in the fluid ("negative buoyancy" is the weight of the body less the weight of the displaced fluid)

t is the time

$T/2$ is the duration of the propulsive force

U_w is the velocity of the sphere at the instant the propulsive force pulse is over

I_w is the net propulsive impulse in the fluid

Similarly, for the sphere launched in a vacuum

$$\int_0^{T/2} (F_a - G_a)dt = MU_a \qquad \text{(Eq. 5)}$$

where the symbols are defined as above, except that launchings are made in a vacuum as indicated by the subscript a.

Assuming F_w and F_a are identical, combining Eq. 4 and Eq. 5 gives

$$\frac{m}{M} = \frac{1}{U_w}\left[U_a + \frac{I_{G_a}}{M} - \frac{I_{G_w}}{M}\right] - 1 \qquad \text{(Eq. 6)}$$

where

$$I_{G_a} = \int_0^{T/2} G_a dt \quad \text{and} \quad I_{G_w} = \int_0^{T/2} G_w dt$$

The velocities U_a and U_w and the mass M can be measured and the impulses I_{G_w} and I_{G_a} can be calculated. Then the quantity $\frac{m}{M}$ can be found by Eq. 6.

The added mass coefficient is then determined by

$$\frac{m}{\rho V} = \left(\frac{m}{M}\right)\left(\frac{M}{\rho V}\right) \qquad \text{(Eq. 7)}$$

where the density ρ is measured and the volume V is calculated using the measured value of the diameter of the sphere.

B. Experimental Equipment and Procedure

1. Fluid Medium

The added mass coefficient determined by Eqs. 6 and 7 is based on launchings in an ideal fluid and in a vacuum. In the experiments air was used as a substitute for a vacuum because it permitted a simplification of the apparatus and because the effects introduced by the air medium were negligible in comparison with the effects to be studied. Tap water was used for the fluid medium in which the added mass of the sphere was measured. Here the effects of fluid viscosity were very small in comparison with the inertial effects but were not negligible, and an analysis was made of these effects allowing a correction to be made for them.

2. Sphere and Suspension

The specifications of the sphere used in the tests follow:

1.0040 ± 0.0001 inches diameter hollow unhardened low carbon steel

Wall thickness, 0.014" approximately

Sphericity, 0.0005"

Weight, 5.6 grams approximately

Mass concentricity best obtainable

Welded assembly

8 R.M.S. or better

No loose material inside ball

High magnetic permeability comparable to 1010 steel

To equip the sphere for the tests it was polished to a mirror finish with diamond dust. Then a very small hole was drilled in it and melted beeswax was poured into it until it was just dense enough to sink in tap water. This density was chosen so that the sphere could be suspended by hanging it on a thread with as little tensile force as possible, and also so that the mass of the sphere was as small as possible in comparison to its added mass to facilitate good precision in the measurements of the latter mass.

After the beeswax had been poured in, it was remelted and allowed to harden with the center of mass located below the center of buoyancy of the sphere so that the hole, the center of buoyancy, and the center of mass were in a straight line. This was done to orient the sphere initially in its rest position so that it would not rotate during its motion in the tests.

Next the hole was sealed with epoxy resin and a small indentation left in the epoxy to allow a knot in the suspension thread to be pushed into the indentation with a pair of tweezers.

The thread suspension was only used in the tests in liquid. For the tests in air the thread was removed and the sphere was placed with its hole vertically upward on a 3/8 inch diameter lucite rod. The top of the rod was made concave and vented by slots at the sides to hold the sphere in its initial position and to eliminate possible air suction effects when the sphere left the rod stand. The purpose of using the rod stand instead of the thread was to eliminate the elasticity effects introduced by the thread suspension. The

effect of gravity acting on the sphere supported initially by the rod stand was on the other hand easily calculated.

3. Test Cylinders

The cylinders used in the tests were made of clear cast acrylic resin. The base of each cylinder was made of a circular lucite plate and fastened by screws to an aluminum ring which was cemented to the bottom of the cylinder. An O ring was used as a seal between the base and the cylinder. The cylinders were carefully checked for longitudinal straightness and for circularity of cross-section and the deviations in both were found negligible. The dimensions of the cylinders are given in Table 2.

Before a cylinder was used in a test it was carefully washed and dried. The region of the cylinder through which light for photographs was to be passed was carefully polished with rotten stone so that there would be no hindrance to light passage. Next the cylinder was placed in a vertical position in a large rectangular clear lucite tank filled with water. The tank is described in detail in Ref. 4. Since lucite and water have nearly equal indices of refraction the diffraction caused by the curved walls of the cylinder was reduced to a negligible quantity because the light reflected from the light source off the sphere to the camera travelled through the water in the cylinder and the water surrounding the cylinder. In any case the curvature was in a direction as to not affect axial displacement measurements.

TABLE 2

Dimensions of the Test Cylinders

Cylinder Number	Measurement Location	I.D. (in.)	O.D. (in.)	Mean I.D.=2a	Mean O.D.	Mean Wall Thickness	$\frac{R_o}{a}$ 2R=1.004"	Approximate Length
10	Top	4.436'	5.004	4.450	4.994	0.272	0.226	4'-5"
	Bottom	4.463	4.988	Inches	Inches	Inches		
5	Top	3.470	4.055	3.480	4.053	0.287	0.289	4'-5"
	Bottom	3.489	4.050					
9	Top	2.456	2.988	2.459	2.996	0.269	0.409	4'-5"
	Bottom	2.462	3.004					
14	Top	1.942	2.469	1.940	2.474	0.266	0.518	4'-5"
	Bottom	1.937	2.474					
13	Top	1.730	2.477	1.718	2.474	0.378	0.585	4'-5"
	Bottom	1.705	2.470					
7	Top	1.482	1.991	1.477	2.000	0.262	0.680	4'-5"
	Bottom	1.471	2.008					
12	Top	1.240	1.982	1.236	1.981	0.373	0.812	4'-5"
	Bottom	1.232	1.979					
11	Test Section	1.109	1.762	-	-	0.327	0.9053	4'-5"

The cylinder was then filled to a height of 40 inches with tap water and the sphere was suspended so that its center was 20 inches below the water surface. This depth of water was found to be adequate for eliminating end effects. That is, the motion of the sphere behaved as though the sphere moved through an infinitely long cylinder. Results of experiments proving that end effects were negligible are included in a later section.

The suspension thread of the sphere previously mentioned in Section B.1 was passed through a hole in the center of an elevation adjusting screw. The thread was brought out of the side of the screw through another hole drilled to meet the center hole and fastened securely to the side of the screw by tape. The adjusting screw was placed in a lucite mount on top of the test cylinder. This mount was constructed so that lateral movement of it could be precisely controlled by a three point lateral suspension consisting of thumb screws threaded through the mount against the cylinder wall. Thus the sphere could be accurately positioned both vertically and laterally in the cylinder. The initial vertical position of the sphere was located precisely by sighting across the top of two horizontal fiducial marks consisting of black tape on both sides of the tank.

The sphere was located midway between the two pieces of tape which were about 2-1/2 feet apart. The proper initial position of the sphere was determined when the tangent of the top of the sphere was in a straight line along the sighting tapes. To locate the sphere center on the axis of the cylinder, vertical black sighting

lines were drawn on a piece of yellow tape and the tape fastened to make a horizontal ring around the cylinder about 3-3/4 inches above the top of the sphere. The sighting lines provided two vertical sighting planes at right angles to each other. To locate the sphere in the center of the cylinder it was only necessary to adjust the suspension mount laterally by the thumb screws so that the sphere suspension thread was on the intersection of both sighting planes at the sighting ring.

Photographs of the apparatus are shown in Figs. 4A, 5A and 6A in Appendix 4.

4. The Electromagnetic Propulsion System

The source of power for launching the spheres consisted essentially of a bank of heavy duty capacitors charged by household power through a high voltage power supply. The capacitors were discharged through a propulsion coil fixed above the sphere. The current flowing produced a magnetic field which acted to accelerate the sphere vertically upward along the axis of the coil. At maximum coil current the approximate magnet intensity was 1200 gauss. Current was allowed to flow in only one direction in the R-L-C circuit formed by the propulsion coil and the capacitors. This was accomplished by a General Electric Ignitron mercury switch in the firing circuit. In this way the sphere was given a force pulse, the time duration of which was about 4 milliseconds. A circuit diagram of the propulsion system is shown in Fig. 3A of Appendix 4.

The initial voltage on the capacitors was maintained constant throughout the tests. This was done by converting the capacitor voltage to frequency by a precision voltage to frequency converter and reading the frequency on a precision frequency counter. By this method the initial voltage on the capacitor was always set to the chosen voltage of 3500 ± 1. The launching coil temperature at the instant before firing was maintained at the same temperature for all tests. In this way the energy supplied to the sphere was constant in all the tests. The coil temperature was measured by means of a thermistor fastened to the coil. The thermistor resistance was measured by a Wheatstone bridge and converted to its corresponding temperature. The temperature chosen was 30°C. This was sufficiently above room temperature to allow the coil to cool rapidly enough after firing so that the waiting time between tests was only about 10 minutes.

The coil itself consisted of 108 turns of 16 gauge copper wire. A diagram of the coil showing the initial position of the sphere is shown in Fig. 1 below.

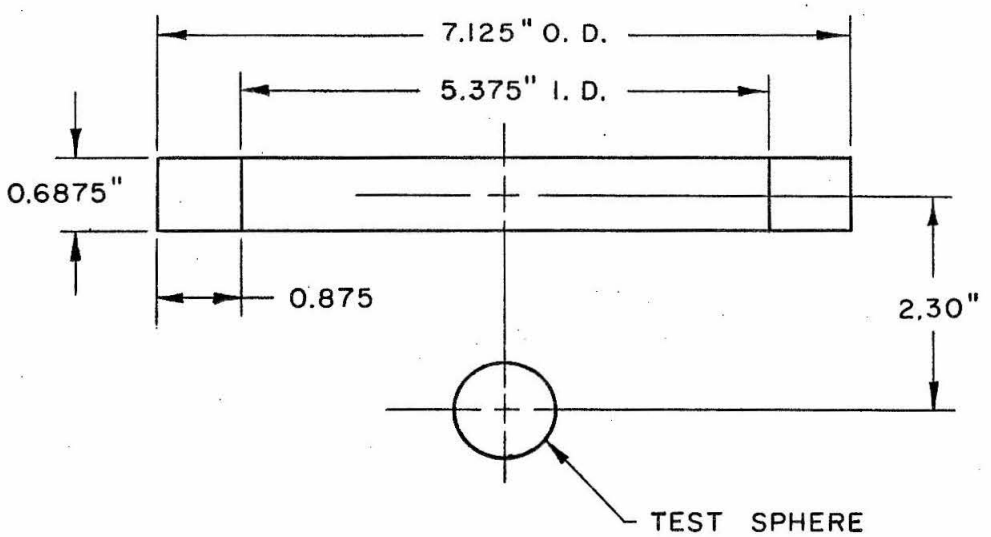

Fig. 1 - Propulsion coil showing initial position of the sphere.

The time duration and magnitude of the current flowing through the propulsion coil was observed by an oscilloscope which was connected to the circuit by means of a pickup coil in which current was induced by passing one of the leads from the capacitor to the propulsion coil through its center. The oscilloscope trace representing the current was photographed by a Polaroid camera. These photographs were used for determining the circuit constants which were necessary in the data analysis.

The launching coil was located and supported as follows: A lucite cylinder with an inside diameter just large enough to allow the coil to fit inside it was positioned in the lucite tank by means of two beams resting on the top of the tank and fastened to the cylinder by brass screws. The beams were permanently located longitudinally and laterally by means of appropriate stops consisting of brass screws in the beams and in the top of the tank. The launching coil was fastened to the bottom end of the lucite cylinder by means of lucite brackets fastened to the cylinder by plastic screws. The test cylinder was located laterally inside the coil so that their two axes coincided. This was done by means of lucite adjusting screws threaded through the coil mount cylinder to contact the test cylinder. The initial position of the center of the sphere below the center of the coil was chosen to be 2.3 inches, a distance which permitted a convenient magnitude of magnetic force to be supplied to the sphere. This distance was maintained throughout the tests with a deviation of not more than 0.01 inches by sighting and adjusting the sphere elevation by the method described in Section B.3.

A close approximation for the electromagnetic force of the accelerating coil on the hollow steel test sphere as a function of space and time is given by the solution of the same problem for a solid steel sphere on the axis of a circular current loop above it.

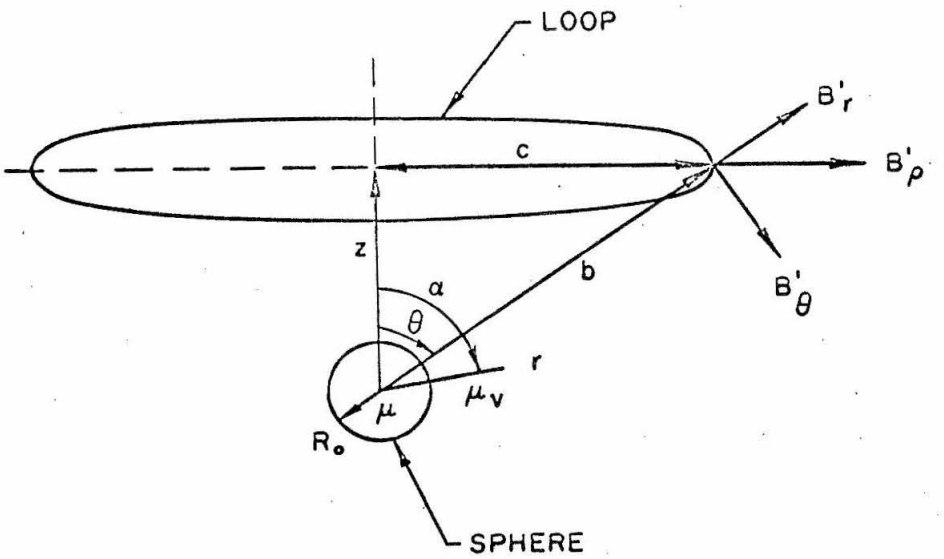

Fig. 2 - Co-ordinate System.

Use is made of a spherical co-ordinate system r, θ, φ with its center coinciding with the center of the sphere and its polar angle θ measured from the top of the sphere on the axis of the loop.

The vector potential of the loop alone for $r < b$ is (see Ref. 5):

$$A_\phi = \frac{\mu_v N I}{2} \sum_{n=1}^{\infty} \frac{\sin \alpha}{n(n+1)} \left(\frac{r}{b}\right)^n P_n^1(\cos \alpha) P_n^1(\cos \theta)$$

where

A_ϕ is the vector potential which has only an azimuthal component

μ_v is the magnetic permeability of air

μ is the magnetic permeability of the sphere

N is the number of turns in the loop

I is the electric current in each turn of the loop

a is the polar angle of the loop

b is the distance from the center of the sphere to the loop

$P_n^1(\cos a)$, $P_n^1(\cos \theta)$ are associated Legendre functions

The vector potential due to the magnetization of the sphere is of the form of A_ϕ but must vanish at infinity.

$$A'_\phi = \frac{\mu_v NI}{2} \sum_{n=1}^{\infty} C_n r^{-n-1} P_n^1(\cos a) P_n^1(\cos \theta) \qquad r > R_o$$

where C_n are constant coefficients.

Inside the sphere the vector potential is

$$A''_\phi = \frac{\mu NI}{2} \sum_{n=1}^{\infty} D_n r^n P_n^1(\cos a) P_n^1(\cos \theta)$$

The boundary conditions are:

At $r = R_o$ $\quad A_\phi + A'_\phi = A''_\phi$ 1 (normal magnetic induction, continuous)

$$\frac{\partial \left[r(A_\phi + A'_\phi) \right]}{\mu_v \partial r} = \frac{\partial (rA''_\phi)}{\mu \partial r}$$ 2 (tangential magnetic field intensity, continuous)

Note:

Curl A = B, B = μH

where

B is the magnetic induction

H is the magnetic field intensity

A is the vector potential

The components of the curl of the vector potential are

$$\text{Curl}_r A = \frac{1}{r \sin\theta}\left[\frac{\partial(\sin\theta\, A_\phi)}{\partial\theta} - \frac{\partial A_\theta}{\partial\phi}\right]$$

$$\text{Curl}_\theta A = \frac{1}{r \sin\theta}\left[\frac{\partial A_r}{\partial\phi} - \sin\theta\,\frac{\partial(rA_\phi)}{\partial r}\right]$$

$$\text{Curl}_\phi A = \frac{1}{r}\left[\frac{\partial(rA_\theta)}{\partial r} - \frac{\partial A_r}{\partial\theta}\right]$$

From boundary condition (1)

$$\frac{\sin\alpha}{n(n+1)}\left(\frac{R_o}{b}\right)^n + \frac{C_n}{R_o^{n+1}} = D_n R_o^n \frac{\mu}{\mu_v} \qquad (1)'$$

From boundary condition (2)

$$\frac{\mu}{\mu_v}\left[\frac{\sin\alpha}{n}\left(\frac{R_o}{b}\right)^n - \frac{C_n^n}{R_o^{n+1}}\right] = D_n(n+1)R_o^n \qquad (2)'$$

Multiplying (1)' by $(n+1)\frac{\mu_v}{\mu}$ - (2)' gives

$$\frac{(\mu_v^2 - \mu^2)\sin\alpha}{n}\left(\frac{R_o}{b}\right)^n + \frac{\left[(n+1)\mu_v^2 + \mu^2 n\right]C_n}{R_o^{n+1}} = 0$$

Then

$$C_n = \frac{(\mu^2 - \mu_v^2)\sin a}{n\left[(n+1)\mu_v^2 + \mu^2 n\right]} \frac{R_o^{2n+1}}{b^n}$$

Thus the vector potential due to the magnetization of the sphere is:

$$A_\phi' = \frac{\mu_v NI}{2} \sum_{n=1}^{\infty} \frac{(\mu^2 - \mu_v^2)\sin a}{n\left[\mu^2 n + (n+1)\mu_v^2\right]} \left(\frac{R_o}{b}\right)^n \left(\frac{R_o}{r}\right)^{n+1} P_n^1(\cos a) P_n^1(\cos \theta)$$

Now to get the vertical component of the force it is necessary to evaluate B_ρ'.

$$B_\rho' = B_r' \sin a + B_\theta' \cos a$$

where

B_ρ' is the radial component of the induction in the plane of the circular loop

B_r' and B_θ' are components of the induction in the spherical co-ordinate system

$$B_r' \sin a = \frac{\partial (\sin a\, A_\phi')}{r\, \partial a}$$

$$B_\theta' \cos a = -\frac{\cos \theta\, \partial (rA_\phi')}{r\, \partial r}$$

Considering only the variable term of A_ϕ':

$$\left[\frac{1}{r^{n+1}} P_n^1(\cos \theta)\right]_\theta = a$$

Note:

$$P_n^1(\cos\theta) = (1 - \cos\theta^2)^{\frac{1}{2}} \frac{dP_n(\cos\theta)}{d\cos\theta}$$

$$= (1 - \cos^2\theta)^{\frac{1}{2}} P'_n(\cos\theta)$$

$$= \sin\theta\, P'_n(\cos\theta)$$

Thus the variable term is

$$\frac{\sin\alpha\, P'_n}{r^{n+1}}(\cos\alpha)$$

Now

$$(B_r \sin\alpha)_v = \frac{1}{r^{n+2}} \frac{\partial\left[\sin^2\alpha\, P'_n(\cos\alpha)\right]}{\partial\alpha}$$

$$= -\frac{\sin\alpha}{r^{n+2}} \frac{\partial}{\partial\cos\alpha}\left[(1 - \cos^2\alpha)\, d\frac{P_n(\cos\alpha)}{d\cos\alpha}\right]$$

$$= \frac{n(n+1)\sin\alpha\, P_n(\cos\alpha)}{r^{n+2}}$$

and

$$(B_\theta \cos\alpha)_v = -\cos\alpha\sin\alpha\, P'_n(\cos\alpha)\frac{\partial}{r\partial r}\left(\frac{1}{r^n}\right)$$

$$= \frac{\cos\alpha\sin\alpha}{r^{n+2}} n\, P'_n(\cos\alpha)$$

Hence

$$(B_r\sin\alpha + B_\theta\cos\alpha)_v = \frac{n\sin\alpha}{r^{n+2}}\left[(n+1)P_n(\cos\alpha) + \cos\alpha P'_n(\cos\alpha)\right]$$

The upward force acting on the sphere is given by

$$F_z = 2\pi c N I B_\rho \qquad \text{at } r = b \qquad \theta = \alpha$$

where

F_z is the component of the magnetic force in the direction of the axis of the loop

c is the radius of the loop.

$$F_z = \frac{u_v \pi c N^2 I^2 \sin^2 \alpha}{b} \sum_{n=1}^{\infty} \frac{\mu^2 - \mu_v^2}{\left[\mu^2 n + (n+1)\mu_v^2\right]} \left(\frac{R_o}{b}\right)^{2n+1} P_n^1(\cos \alpha)$$

$$\left[(n+1)P_n(\cos \alpha) + \cos \alpha \, P_n'(\cos \alpha)\right]$$

The first term approximation of the solution is

$$F_z \approx \frac{3\mu_v \pi c N^2 I^2 \sin^2 \alpha}{b} \frac{\mu^2 - \mu_v^2}{\mu^2 + 2\mu_v^2} \left(\frac{R_o}{b}\right)^3 \left(\frac{c}{b}\right)^3 \frac{z}{b}$$

$$\approx \frac{3\pi N^2 I^2 \mu_v (\mu^2 - \mu_v^2)}{\mu^2 + 2\mu_v^2} \frac{c^4 R_o^3 z}{b^8}$$

This approximation neglects $\left(\frac{R_o}{b}\right)^5$ compared with $\left(\frac{R_o}{b}\right)^3$

For the coil and sphere used in the experimental tests

$R_o = \frac{1.004}{2}$ inches, $z_o = 2.30$ inches, and $c = 3.03$ inches.

So then

$$\left(\frac{R_o}{b}\right)^2 = \frac{R_o^2}{z_o^2 + c^2} = 0.0347 .$$

Therefore the second term of the series for F_z is only 3.47 percent of the first term. This means physically that the error in the force by assuming that all of the magnetic material of the solid sphere is concentrated at its center is only 3.47 percent.

For a given loop and solid sphere both in air the force can be written

$$F_z \approx \frac{K' z I^2}{(c^2 + z^2)^4}$$

where

$$K' = \frac{3\pi N^2 \mu_v (\mu^2 - \mu_v^2)}{\mu^2 + 2\mu_v^2} = \text{constant.}$$

For a hollow sphere the first term approximation for force as a function of space and time is about as good. However, the value of the constant K' is different.

Thus for the hollow test sphere and the propulsion coil used in the experiments the magnetic force is given by

$$F_z \approx \frac{K z I^2}{(R_o^2 + z^2)^4} , \quad K \text{ constant} \qquad \text{(Eq. 8)}$$

The current flowing in the series R-L-C circuit of the propulsion system is given by

$$I = I_o e^{-\alpha t} \sin \omega t \qquad \text{(Eq. 9)}$$

where

I is the current flowing at a given time

I_o is the current constant

$\alpha = \frac{R}{2L}$ is the damping constant

R is the total resistance of the energizing circuit

L is the total inductance of the circuit, and

ω is the natural frequency of the circuit.

Substituting Eq. 9 into Eq. 8 gives the magnetic force on the sphere as a function of space and time.

$$F_z \approx \frac{Kze^{-2\alpha t} \sin^2 \omega t}{(c^2 + z^2)^4} \qquad \text{(Eq. 10)}$$

Equation 10 is derived on the assumption that the motion of the sphere producing eddy currents has negligible effect on the strength of the magnetic force. This assumption was shown to be valid by observing that a non-magnetic sphere placed in the initial position of the tests did not move in the rapidly changing magnetic field of the propulsion coil, and noting that the field changed much more rapidly here than it did due to motion of the sphere.

The current and force functions of time from Eqs. 9 and 10 respectively are plotted on the following page in Fig. 3. The force function is plotted for z held constant. A check was made

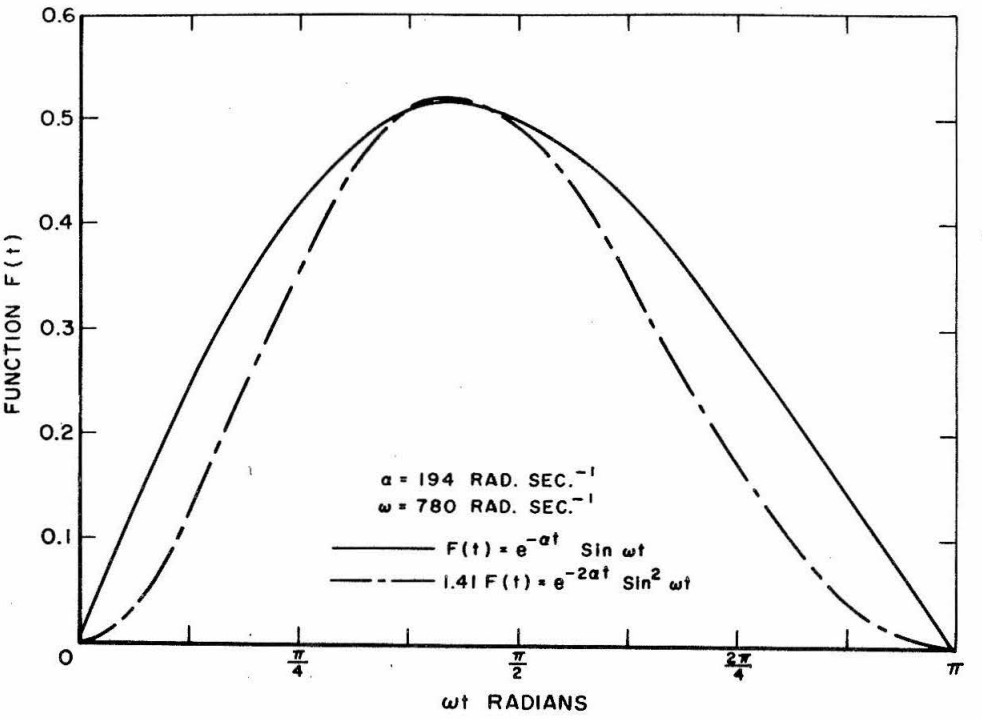

Fig. 3 - Theoretical values of F(t)

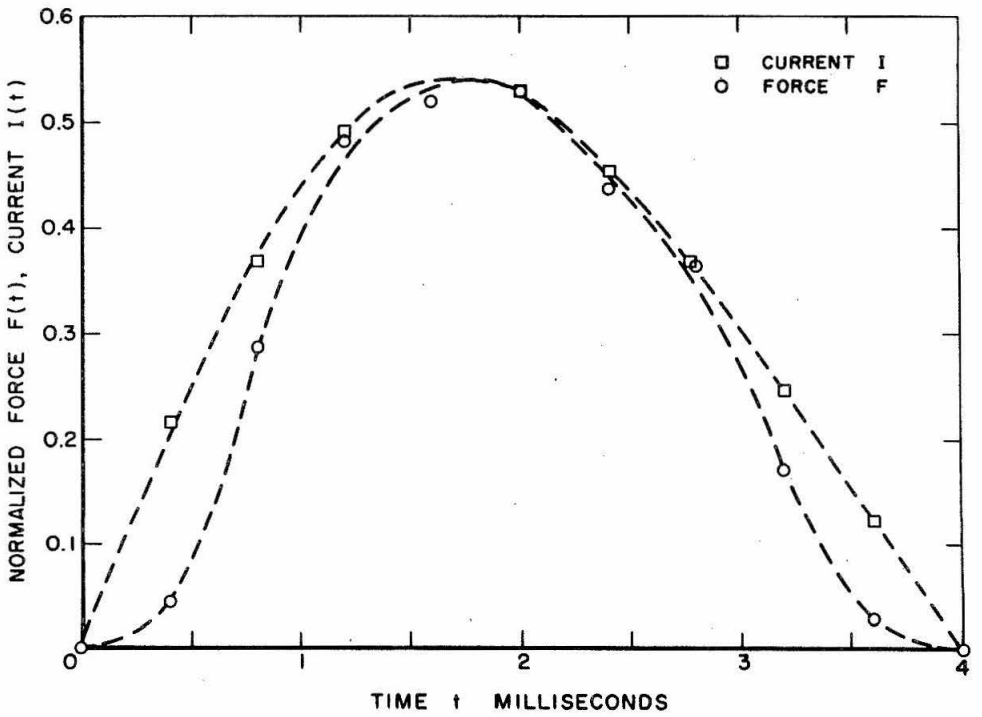

Fig. 4 - Experimental current and force functions

to show that the experimental propulsion apparatus actually obeyed these functions. The current and force as functions of time determined experimentally are shown in Fig. 4. These functions were taken from the oscilloscope record of the experimental tests shown in Fig. 7A of Appendix 4.

To measure the force acting on the sphere as a function of time, the propulsion coil was suspended by very long weak springs. The springs were weak enough so that the dynamic spring force was negligible in comparison to the inertial reaction force of the coil. Also, the period of oscillation of the spring mass system was much longer than the time duration of the magnetic force pulse. This made it possible to obtain approximately the magnetic force by measuring the acceleration of the coil and using the simple relation

$$F = M_c a_c = M_s a_s$$

where

s = sphere

c = coil.

The coil acceleration was measured using the oscilloscope and accelerometers attached to the coil.

The current in the coil was measured at the same time as the force using the oscilloscope and a pickup coil through which one of the leads to the propulsion coil was passed.

5. The Photographic Technique for Measuring the Motion of the Sphere

The photographic technique for measuring the motion of the sphere is described in great detail in Ref. 6. It will only be described briefly here.

The method for measuring position as a function of time consisted essentially of using photographs of the virtual image or "high light" produced in a sphere by a stroboscopic point-light source. The range and number of sphere positions to be observed over the exposure sequence were adjusted by setting the frequency and gating the number of flashes. A time-delay generator, adjustable to one microsecond, triggered the flash sequence at the appropriate instant after the propulsion coil was energized. The frequency used was set and maintained throughout all tests by a variable frequency oscillator with a precision frequency counter readout. The frequency used was 2000 ± 1 flashes per second. The time delay used was one-half millisecond for all tests. Using this time delay the first two dots on the displacement-time photographs were conveniently individually distinguishable. A displacement-time photograph is shown in Fig. 8A of Appendix 4.

To obtain the data the sphere initial position was carefully checked and the energizing capacitors were charged to about 3510 volts, after which the room was darkened. Then the capacitor voltage was allowed to leak off until the precision counter monitoring

it read 3500 volts, at which point the camera shutter was opened and the launching circuit and stroboscopic lamp actuated, after which the camera shutter was closed.

The images produced on the photographs were circular and sharp and the author's experience indicated that the cross hairs of the precision measuring microscope described in the sequel was centered on them with a precision of ± 5 microns for good highlights and ± 2 microns for very good highlights. The position of the highlight images was measured by means of a measuring microscope constructed by David W. Mann, Precision Instruments, Lincoln, Massachusetts. This instrument had a measurement capacity of 200 millimeters in the abscissa and 30 millimeters in the ordinate directions. The readout was one micron. The stage and cross hairs were rotatable and both were provided with circular angular scales with verniers so that the angles were readable to one minute.

C. Results

1. Obtaining Velocity from Displacement-Time Photographs

For calculating the added mass of the sphere in the cylinder using Eqs. 6 and 7 the velocities U_a and U_w were required. These were obtained from the displacement-time photographs as follows. The time duration of the force pulse was determined from photographs of the oscilloscope trace of the current in the propulsion coil and was 4.02 ± 1 milliseconds for all the tests. The first dot

occurred between 1/2 and 1 millisecond after current started to flow in the coil. The exact time at which the first dot occurred was measured with a precision frequency counter. The accuracy of the oscilloscope time scale was checked using the fact that the time interval between light flashes was known to be 0.5000 + 0.0005 milliseconds. The current trace on the oscilloscope was interrupted at the time of the light flashes. The first dot after the force pulse was over on the time-displacement photographs was then found either by looking at the oscilloscope trace or by counting the dots after the time of the initial dot recorded by the precision counter. The velocity as a function of time during the coasting period after the propulsive force stopped was then determined by dividing the distance between adjacent dots by the time interval between them. Next a straight line was fitted by the method of least squares through at least the first ten velocity-time points in the coasting regime and the velocity of the sphere at the end of the force pulse was determined by the intercept of this straight line at the time of the end of the force pulse. This method was found to give uniform reproducible results. The number of points used in the velocity time line was kept small enough so that the sphere had not travelled over 0.40 inches from its launching position. A check was made of the linearity of the velocity-time function by means of fitting straight lines to a larger and smaller number of points during the coasting regime and comparing these lines to the lines actually used. Only negligible differences in slope and intercept were found. The velocities obtained by this method are

shown in Table 4 of Section 7.

The mean velocity versus time during the coasting regime for all the cylinders is shown in Figs. 10A through 17A in Appendix 4. This mean velocity was obtained by averaging the velocities at each corresponding time point for all the runs made. These graphs serve only as a means of looking at the general motion of the sphere during the coasting regime. They played no direct part in the measurement of the added mass.

2. Correction for Gravitational Force

The sphere was launched vertically upward in the earth's gravitational field and the gravitational effect was determined as follows.

Shots in Air

The net force acting to accelerate the sphere was

$$F = F_a - Mg$$

where g is the acceleration due to gravity.

The ball begins to move at time T_1 when $F_a = Mg$. The total impulse imparting momentum to the sphere was

$$\int_{T_1}^{T/2} (F_a - Mg)\, dt$$

where $T/2$ was the duration of the propulsive force pulse.

The total impulse imparting momentum to the sphere in the

absence of gravity would have been

$$\int_0^{T/2} F_a \, dt$$

The negative impulse imparted to the sphere by gravity is found by subtracting the first integral from the second. That is

$$I_{G_a} = \int_0^{T/2} F_a \, dt - \int_{T_1}^{T/2} (F_a - Mg) \, dt$$

or

$$I_{G_a} = \int_0^{T_1} F_a \, dt + Mg \left(\frac{T}{2} - T_1\right) \qquad \text{(Eq. 11)}$$

The time T_1 was observed experimentally to be less than $1/4$ m.s. $<<\frac{T}{2} \approx 4$ m.s. Then the following approximate relationship between the impulse and momentum holds for calculating T_1:

$$\int_0^{T/2} (F_a - Mg) \, dt \approx M U_a \qquad \text{(Eq. 12)}$$

Then using Eq. 10 and neglecting the spacial variation of the magnetic field, justified by the short distance the sphere moved, Eq. 12 becomes

$$\int_0^{T/2} (Ke^{-2\alpha t} \sin^2 \omega t - Mg) \, dt = M U_a \qquad \text{(Eq. 13)}$$

Performing the integration gives

$$M U_a = \frac{K\omega}{4(\omega^2 + a^2)} \left[\frac{\omega}{a} (1 - e^{-at}) \right] - Mg\frac{T}{2} \qquad \text{(Eq. 14)}$$

This equation can be solved for $\frac{K}{M}$ since all of the other constants are known. The values of a, ω, and T and the method for finding them are found in Sections IV.A and IV.B. Thus

$$\frac{K}{M} = 79660 \text{ in.sec.}^{-2}$$

Since T_1 is less than 1/4 millisecond the magnetic force in the time $0 < t < T_1$ can be written as

$$F_a \approx K \sin^2 \omega t \qquad 0 < t < T_1$$

so that T_1 can be found from

$$K \sin^2 \omega T_1 = Mg$$

or

$$\sin \omega T_1 = \sqrt{\frac{Mg}{K}}$$

from which $T_1 = 0.0833$ milliseconds.

Then using Eq. 11

$$\frac{I_{G_a}}{M} = \int_0^{T_1} K \sin^2 \omega t \, dt + g \left(\frac{T}{2} - T_1\right)$$

Also

$$\int_0^{T_1} K \sin^2 \omega t \, dt \approx \frac{K}{\omega} \int_0^{T_1} \left(\omega t - \frac{\omega t^3}{6}\right)^2 d(\omega t)$$

$$\approx \frac{K(\omega T_1)^3}{3\omega} = 0.005 \text{ in. sec.}^{-1}$$

Now $\frac{T}{2}$ = 4.02 milliseconds and g = 386.4 in. sec.$^{-2}$.

Thus the reduction in velocity caused by gravitational force during the propulsive force period is

$$\frac{I_{G_a}}{M} = 1.51 \text{ in. sec.}^{-1} \qquad \text{(Eq. 15)}$$

Shots in Water

As was previously pointed out the sphere was nearly the same density as the water and only a very small net downward force was exerted by gravity. For this reason T_1 and the effect of initial string tension were neglected.

The downward force exerted was

$$F = (M - \rho V) g$$

The impulse of this force during the pulse period was

$$I_{G_w} \approx \int_0^{T/2} F \, dt = \int_0^{T/2} (M - \rho V) g \, dt$$

Performing the integration and dividing both sides of the equation by M for convenience later in calculating added mass there results

$$\frac{I_{G_w}}{M} = (1 - \frac{\rho V}{M}) g \frac{T}{2}$$

Now

$$M = 9.3055 \text{ gm.}$$

$$\rho = 0.9980 \text{ gm. cm.}^{-3} \text{ for water at } 21^{\circ}\text{C}$$

$$V = 8.6835 \text{ cm.}^{3}$$

Thus

$$\frac{I_{G_w}}{M} = 0.106 \text{ in. sec.}^{-1} \qquad \text{(Eq. 16)}$$

3. Calculation of Added Mass and Comparison to Theoretical Value

A sample calculation for the added mass of the sphere in the cylinder with sphere to cylinder ratio $\frac{R_o}{a} = 0.226$ (Table 2) follows.

$$\frac{m}{M} = \frac{1}{U_w}\left[U_a + \frac{I_{G_a}}{M} - \frac{I_{G_w}}{M}\right] - 1$$

$$= \frac{82.29 + 1.51 - 0.11}{55.73} - 1 = 0.5017$$

The values of U_a and U_w are the mean values taken from Table 4 in Section III. C. 7.

$$\frac{M}{\rho V} = \frac{9.3055 \text{ gm.}}{(0.9980 \text{ gm. cm.}^{-3})(8.6835 \text{ cm.}^{3})} = 1.0737$$

Then

$$\frac{m}{\rho V} = \left(\frac{m}{M}\right)\left(\frac{M}{\rho V}\right) = (1.0737)(0.5017)$$

from Eq. 8, giving

$$\frac{m}{\rho V} = 0.5387$$

The theoretical value is found using Table 1. From Table 1:

$$\text{For } \frac{R_o}{a} = 0.2 \qquad \frac{m}{\rho V} = 0.5096$$

$$\text{For } \frac{R_o}{a} = 0.3 \qquad \frac{m}{\rho V} = 0.5330$$

Using linear interpolation to obtain the added mass ratio for $\frac{R_o}{a} = 0.226$, we have

$$\frac{m}{\rho V} = 0.5096 + (0.5330 - 0.5096)\left(\frac{0.026}{0.100}\right) = 0.5157$$

The ratio of the experimentally determined added mass ratio to the corresponding theoretical value is

$$\frac{m_{ex}}{m_{th}} = \frac{0.5387}{0.5157} = 1.0446 \ .$$

The experimentally determined added mass and the corresponding theoretical values were calculated in the same manner for all of the cylinders and the results are tabulated in Table 5 in Section III. C. 7.

4. Statistical Significance of Results

It is also of interest to obtain for tests of statistical significance the limits corresponding to various levels of probability for the added mass ratios. Unfortunately, small sample

theory is unavailable for making such tests directly and it will be necessary to use approximate theory. Let the population (universe) average values of $\overline{U}_{ac}$ and $\overline{U}_{w}$ be $\tilde{U}_{ac}$ and $\tilde{U}_{w}$ respectively. Let the standard errors of the average values be $\overline{\sigma}_{a}$ and $\overline{\sigma}_{w}$. Let the experimentally obtained ratio $\overline{U}_{ac}/\overline{U}_{w} = \ell$ where

$$U_{ac} = U_{a} + \frac{I_{G_a}}{M} - \frac{I_{G_w}}{M},$$

and the population (universe) ratio be λ.

Then from statistical theory for large samples (Ref. 7)

$$\overline{\sigma}_{\ell}^{2} = \lambda^{2}\left[\frac{\overline{\sigma}_{w}^{2}}{\tilde{U}_{w}^{2}} + \frac{\overline{\sigma}_{a}^{2}}{\tilde{U}_{ac}^{2}}\right] \qquad \text{(Eq. 17)}$$

In Eq. 17 it will be necessary to make some approximations. We do not have any a priori knowledge of the population or universe parameters, but fortunately from Table 5 we observe that the variation of individual (and hence average) values is small compared to their actual values. Consequently we may use the experimental parameters in place of the universe parameters in Eq. 17 without introducing appreciable error. That is, we use

$$\overline{\sigma}_{\ell}^{2} = \ell^{2}\left[\frac{\overline{\sigma}_{w}^{2}}{\overline{U}_{w}^{2}} + \frac{\overline{\sigma}_{a}^{2}}{\overline{U}_{a}^{2}}\right]$$

to estimate $\overline{\sigma}_{\ell}$. Since the samples are small, standard errors are computed by means of the well known formula

$$\bar{\sigma} = \sqrt{\sum_{i=1}^{N} \frac{(X_1 - \bar{X})^2}{N(N-1)}}$$

where N is the number of items in the sample. Then from Eq. 6 the standard error in the added mass can be found. That is

$$\frac{m_{ex}}{M} = \frac{U_{ac}}{U_w} - 1 = \ell - 1$$

so

$$\frac{m_{ex}}{m} = (\ell - 1)\frac{M}{m}$$

where m_{ex} is the experimentally determined added mass. Then the standard error in m_{ex}/m is given by

$$(\ell + \sigma_\ell - 1)\frac{M}{m} - (\ell - 1)\frac{M}{m} = \frac{\sigma_\ell M}{m} \qquad \text{(Eq. 18)}$$

The standard errors and the confidence limits for 2 and 3 times the standard error corresponding to probabilities of 0.9546 and 0.9973 respectively that added mass will fall within these limits are shown in Table 5 in Section C.7.

5. Correction Due to Magnetic Impulse Differences

A small correction due to differences between the net propulsive impulses imparted to the sphere in the tests in air and in water was necessary. The impulse imparted to the sphere in the tests in water was the lower impulse because the virtual mass of the

sphere in water was greater by approximately the amount of its added mass in this medium. This higher virtual mass in water prevented the sphere going as far into the field of the coil as it did in air. For the distance covered by the sphere during the propulsive force period the spatial variation of the magnetic field was an increasing function of sphere displacement. Hence since the sphere did not go as far into the field of the coil for tests in water, the net propulsive impulse applied to it was less than for the tests in air. The spatial function of the magnetic field is shown in Fig. 5.

Instead of Eq. 6 which assumes that the impulses are equal, a new equation in which they are not quite equal is necessary. That is

$$I_{F_w} = (M + m)\,U_a + I_{G_w} \quad \text{and} \quad I_{F_a} = M\,U_a + I_{G_a}$$

as before, but since I_a and I_w are not equal the following more complicated equation is obtained from the above two equations instead of Eq. 6.

$$\frac{m}{M} = \frac{1}{U_w}\left[\frac{U_a + \frac{I_{G_a}}{M}}{\left(\frac{I_{F_a}}{I_{F_w}}\right)} - \frac{I_{G_w}}{M}\right] - 1 \qquad \text{(Eq. 19)}$$

The only quantity which does not appear in Eq. 6 is the ratio

$$\frac{I_{F_a}}{I_{F_w}}$$

which was evaluated by using Eq. 10 and the displacement time photographs.

From Eq. 10 the spatial variation of the magnetic field of

the propulsion coil is

$$f(z) = \frac{z}{(c^2 + z^2)^4}$$

Expanding this in a Taylor series about z_o, the initial position of the sphere, and keeping only the first two terms, which is a good approximation because the displacement of the sphere was small in the field of the coil, gives

$$f(z - z_o) = f(z_o) + f'(z_o)(z - z_o) + \ldots .$$

$$= f(z_o) + \frac{c^2 - 7z_o^2}{(c^2 + z_o^2)^5}(z - z_o)$$

In the experiments the radius of the propulsion coil was $c = 3.03$ inches and $z_o = 2.3$ inches. Then

$$f(z - z_o) = 5.246 - 4.3903(z - z_o) \quad \times 10^{-5}\text{inches}^{-7}$$

where $z - z_o$ is in inches.

Let the displacement from the initial position $z - z_o = -S(t)$. Then $S(t)$ is the displacement of the sphere in inches measured upward from its initial position.

$$f(z - z_o) = (5.246 + 4.3903S) \times 10^{-5}\text{inches}^{-7} \qquad \text{(Eq. 20)}$$

Substituting the approximate space function given by Eq. 20 for the exact space function in Eq. 10 and integrating over the pulse time

gives the impulse due to the magnetic force. That is

$$I_F = \int_0^{T/2} F_M dt = K \times 10^{-5} \int_0^{T/2} (5.246 + 4.3903S)\, e^{-2\alpha t} \sin^2 \omega t \, dt$$

or

$$I_F + 1.195\, K' \int_0^{T/2} e^{-2\alpha t} \sin^2 \omega t \, dt + K' \int_0^{T/2} S(t) e^{-2\alpha t} \sin^2 \omega t \, dt$$

where K' is a dimensionless constant.

$$\int_0^{T/2} e^{-2\alpha t} \sin^2 \omega t \, dt = \frac{\omega^2 (1 - e^{-\alpha t})}{4(\omega^2 + \alpha^2)\alpha} = 9.894 \times 10^{-4} \text{sec.}$$

The circuit parameters ω, α, and T remained for all practical purposes constant in all tests and the values used in the preceding integral were measured by the method outlined in Section IV. B. The mean values of the measurements taken from sixteen launchings were

$$\alpha = 185 \text{ rad. sec.}^{-1}$$

$$\omega = 781 \text{ rad. sec.}^{-1}$$

$$T/2 = 4.02 \times 10^{-3} \text{sec.}$$

Now the impulse integral can be written

$$\frac{I_F}{K'} = 11.823 \times 10^{-4} + \int_0^{T/2} S(t)\, e^{-2\alpha t} \omega t \, dt \text{ in. sec.} \qquad \text{(Eq. 21)}$$

Equation 21 is a convenient form for determining the required quantity

$$\frac{I_{F_a}}{I_{F_w}} \quad .$$

The integral in Eq. 21 was readily solved numerically using Simpson's rule. The displacement S(t) was determined using the same time displacement photographs used for finding the velocities at the end of the force period. The value so determined was the mean of the time displacement values determined from all of the seven or eight repeated trials. Curves plotted from these values are shown in Figs. 18A, 19A and 20A of Appendix 4.

Since the first dot on the photographs occurred approximately 0.75 milliseconds after current began to flow in the propulsion coil it was necessary to make a calculation to determine the displacement of the sphere during this first 0.75 milliseconds of time. This displacement was very small in comparison to the total distance travelled during the pulse period and was therefore easily accounted for by approximate methods.

Using the same approximation for the force pulse as in Section III. C. 2, the velocity of the sphere in air at time t ,

$$T_1 \leq t \leq 0.75 \text{ m.s.}$$

is given by

$$U(t) = \int_{T_1}^{t} K \sin^2 \omega t \, dt - g(t - T_1) = \frac{K}{\omega} \left[\left(\frac{\omega t}{2} - \frac{\sin 2\omega t}{4} \right) \right.$$

$$\left. - \left(\frac{\omega T_1}{2} - \frac{\sin 2\omega T_1}{4} \right) \right] - g(t - T_1)$$

This equation is then integrated to give the displacement S at time t = 0.75 milliseconds. That is

$$S(t) \approx \frac{K}{\omega^2} \left\{ \left[\frac{(\omega t)^2}{4} + \frac{\cos 2\omega t}{8} \right]_{\omega T_1}^{\omega t} - \left[\left(\frac{\omega T_1}{2} - \frac{\sin 2\omega T_1}{4} \right) \omega t \right]_{\omega T_1}^{\omega t} \right\}$$

$$- \frac{g}{2} (t^2 - T_1^2) - g(t - T_1) T_1 \qquad \text{(Eq. 22)}$$

Substituting the values of K, ω and T_1 as in Section III. B. 2, the value of S at time t = 0.75 milliseconds is determined. This gives S = 0.0017 inches for t = 0.75 m. s.

The evaluation of the integral in Eq. 21 was facilitated by the following table.

Evaluation of Impulse Integral

Elapsed Time t m.s.	$e^{-\alpha t}\sin^2 \omega t$	S' Inches	$S = S' + 0.0017$ Inches	$Se^{-2\alpha t}\sin^2 \omega t$	For Simpson's Rule
0.75	0.2314	0	0.0017	0.00039	$y_o = 0.00039$
1.25	0.4318	0.0075	0.0092	0.00397	$4y_1 = 0.01588$
1.75	0.5014	0.0225	0.0242	0.01213	$2y_2 = 0.02426$
2.25	0.4196	0.0455	0.0472	0.01981	$4y_3 = 0.07924$
2.75	0.2470	0.0762	0.0779	0.01924	$2y_4 = 0.03848$
3.25	0.0967	0.1129	0.1146	0.01108	$4y_5 = 0.04432$
3.75	0.0112	0.1527	0.1546	0.00173	$y_6 = 0.00173$
					$\sum = 0.20430$

Then, using Simpson's rule

$$\int_{t}^{3.75 \times 10^{-3}} Se^{-2at}\sin^2\omega t\, dt = \frac{h}{3}(y_o + 4y_1 + 2y_2 + 4y_3 + \ldots 4y_{2n-=} + y_{2n})$$

$$= \frac{(5 \times 10^{-3})(0.20430)}{3} = 0.3405 \times 10^{-4} \text{ in. sec.}$$

The value of the integral from $t = 3.75$ m.s. to the end of the pulse period was

$$\int_{3.75 \times 10^{-3}}^{4.023 \times 10^{-3}} Se^{-2at}\sin^2\omega t\, dt \approx (\frac{y_6}{2})(\frac{\Delta t}{2}) = 0.00118 \times 10^{-4} \text{ in. sec.}$$

The value of the integral from the start of the force pulse to $t = 0.75$ m.s. was

$$\int_{0}^{0.75 \times 10^{-3}} Se^{-2at}\sin^2\omega t\, dt \approx (\frac{y_o}{2})(\frac{2\Delta t}{3}) = 0.00098 \times 10^{-4} \text{ in. sec.}$$

Then adding the three integrals gives

$$I_1 = \int_{0}^{T/2} Se^{-2at}\sin^2\omega t\, dt = 0.3427 \times 10^{-4} \text{ in. sec.}$$

The same treatment applied to the tests in water in the largest cylinder (4.45" I.D.) gave

$$I_1 = \int_{0}^{T/2} Se^{-2at}\sin^2\omega t\, dt = 0.2410 \times 10^{-4} \text{ in. sec.}$$

Then using Eq. 21 we obtain the ratio of the impulse in air to the impulse in water in the largest cylinder

$$\frac{I_{F_a}}{I_{F_w}} = \frac{11.823 + 0.3427}{11.823 + 0.2410} = 1.0084$$

The impulses for the smaller cylinders were easily calculated by noting that the integral I_1 was approximately proportional to the total displacement S during the pulse period. That is

$$I_1^{(2)} = \frac{S^{(2)}}{S^{(1)}} I_1^{(1)} \qquad \text{(Eq. 23)}$$

The following table gives the impulse ratio based on Eq. 23 and the I_1 integrals for the largest cylinder. Here the displacement S' which neglects the very small displacement during the first 0.75 milliseconds was used instead of S for convenience.

Table 3

Ratio of Propulsive Impulse for Sphere in Air to Propulsive Impulse for Sphere in Water

Cyl. I.D. Inches	Displacement S' During Pulse Period	I_1 In. Sec.	$\frac{I_{F_a}}{I_{F_a}}$
4.450	0.1053	0.2411×10^{-4}	1.0084
3.480	0.1016	0.2326	1.0091
2.459	0.1010	0.2313	1.0093
1.940	0.0958	0.2194	0.0103
1.718	0.0916	0.2097	1.0111
1.477	0.0776	0.1777	1.0138
1.236	0.0621	0.1422	1.0168
1.109	0.0399	0.0914	1.0211

Now Eqs. 19 and 11 are used to calculate the added mass ratio. The results are tabulated in Table 6, Section III. C. 7.

The spacial variation of the magnetic force is shown in Fig. 5. z_o is the initial position of the sphere. z_a and z_w are the positions of the sphere at the end of the force pulse in air and water in the 4.45 inch I.D. cylinder respectively.

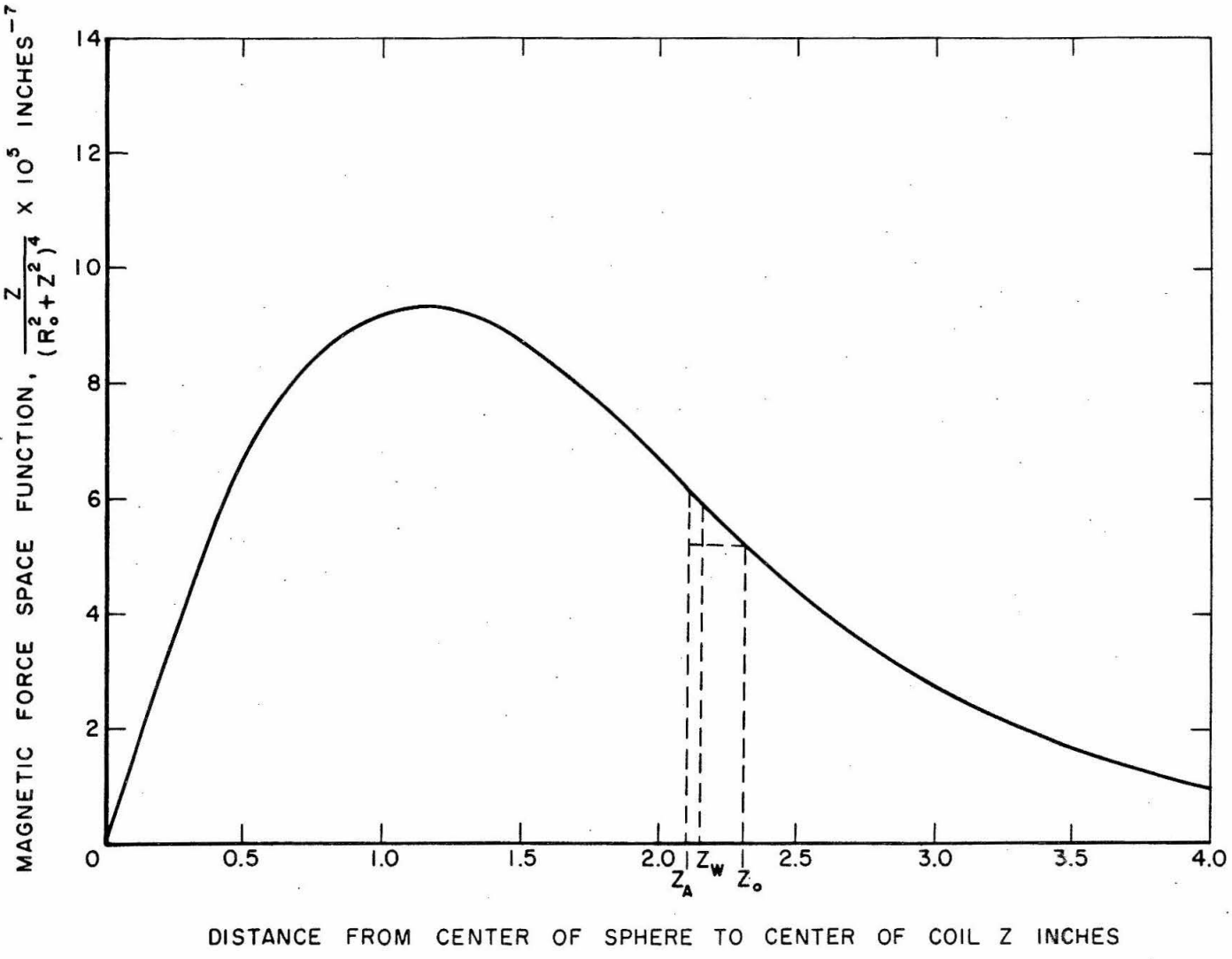

Fig. 5 - Spacial variation of magnetic propulsive force

6. Surface Effects

For the theoretical evaluation of the added mass for an ideal fluid the cylinders were assumed to be infinitely long. For the experimental evaluation of this added mass a column of water about 40 inches high was used with the sphere initial position near the middle of this column. A series of tests was made to show that the effects of the free surface above the sphere and the bottom of the cylinder below the sphere were negligible. In other words, the added mass measured represented the added mass for infinitely long cylinders.

The tests consisted of a series of measurements of added mass for various heights of the water column above the initial position of the sphere. The depth of the sphere center was varied from a minimum of one inch to a maximum of 19 inches, the latter depth corresponding to the standard test depth used for all the cylinders. These measurements were done only in the largest cylinder. It was discovered that the 19 inch depth used was more than adequate. On the other cylinders a visual check for the motion of the free surface was made, as an extra precaution. No motion of the surface was observed during the tests.

The variation of added mass with depth is shown in Table 8, Section III. C. 7, and Fig. 8. Also shown in this section are results of some tests for vertical motion of the sphere toward the water surface in a large tank giving no wall effects.

Table 4

Velocity of Sphere at the End of the Acceleration Regime
for Tests in Water in Various Cylinders and Tests in Air

Cylinder I.D. (inches)	4.450	3.480	2.459	1.940	1.718	1.477	1.236	1.109	Tests in Air
	56.18	54.93	53.74	49.38	47.03	42.53	30.98	20.76	82.43
Velocity at end of acceleration regime (in./sec.)	55.58	55.04	53.85	50.17	47.56	42.57	31.51	20.07	82.43
	55.66	54.75	52.98	49.79	47.77	42.59	31.64	19.88	82.66
	55.80	54.98	53.65	49.95	47.06	43.17	31.38	20.25	82.30
	55.35	54.71	53.26	49.88	46.63	42.35	30.99	20.20	82.12
	55.75	54.93	53.10	50.01	47.40	42.09	31.04	20.50	82.10
	55.80	54.63	52.96	50.16	46.68	41.85	31.16	20.33	81.99
		54.75			47.03	42.36	31.15	20.20	
Mean sphere velocity U_w, U_a (in. $sec.^{-1}$)	55.731	54.840	53.363	49.906	47.145	42.439	31.231	20.273	82.29
*b in. $sec.^{-1}$ $int.^{-1}$	-0.081	-0.094	-0.079	-0.064	-0.083	-0.072	-0.065	-0.180	
*Δt m.s.	4-1/2	5	5	5-1/2	6	7	5	2-1/2	

* b is mean slope of velocity-time line after force pulse
int. is time interval of 1/2 millisecond
Δt is time over which straight line was fitted

Table 5

Effect of Cylinder Diameter On the Added Mass of a 1.004 Inch Diameter Sphere Accelerated Axially from Rest in Water

Cylinder I.D. (inches)	Theoretical Added Mass $\frac{m_{th}}{\rho V}$	Experimental Added Mass $\frac{m_{ex}}{\rho V}$	Ratio $\frac{m_{ex}}{m_{th}}$	Standard Error in $\frac{m_{ex}}{m_{th}}$	Confidence Limits	
				$\sigma_m \times 10^2$	0.9546	0.9973
4.450	0.5157	0.5387	1.0446	±0.0063	0.0126	0.0189
3.480	0.5648	0.5302	1.0653	0.0044	0.0088	0.0132
2.459	0.5883	0.6101	1.0370	0.0082	0.0164	0.0264
1.940	0.6924	0.7265	1.0492	0.0060	0.0199	0.0180
1.718	0.7907	0.8320	1.0522	0.0034	0.0069	0.0103
1.477	1.0172	1.0434	1.0258	0.0075	0.0150	0.0225
1.236	1.7177	1.8029	1.0496	0.0055	0.0110	0.0165
1.109	2.9388	3.3280	1.1324	0.0057	0.0114	0.0171
Mean for 7 largest cylinders			1.0462			

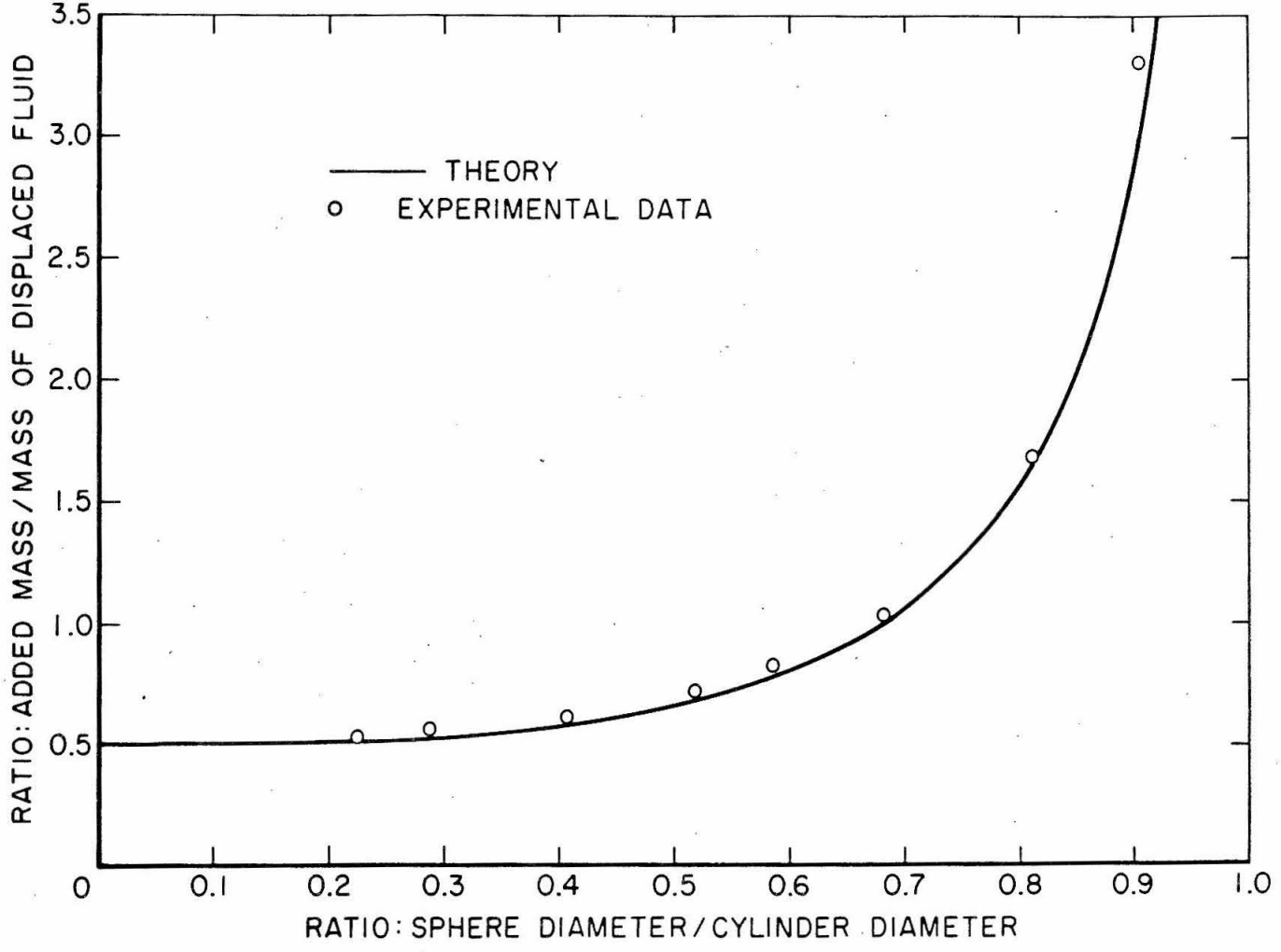

Fig. 6 - Added mass of a sphere accelerated along the axis of a long circular cylinder

Table 6

Added Mass from Table 5 Corrected for Difference Between Impulse in Water and Air

Cylinder I.D. (inches)	Experimental Added Mass $\frac{m_{ex}}{\rho V}$	Ratio $\frac{m_{ex}}{m_{th}}$
4.450	0.5251	1.0182
3.480	0.5499	1.0372
2.459	0.5945	1.0105
1.940	0.7084	1.0231
1.718	0.8111	1.0258
1.477	1.0146	0.9974
1.236	1.7554	1.0219
1.109	3.2661	1.1119
Mean for 7 largest cylinders		1.0192

Table 7

Added Mass of a 1.004 Inch Diameter Sphere
In a Large Tank of Water for Various Depths
of the Sphere Below the Surface

Initial Depth of Sphere Center h inches	Added Mass Coefficient $\frac{m}{\rho V}$	Added Mass at h Compared to Added Mass at ∞ $\frac{m_h}{m_\infty}$
1/2	0.3581	0.7162
5/8	0.4263	0.8526
3/4	0.4822	0.9644
7/8	0.4878	0.9756
1	0.4993	0.9986
1-1/8	0.5028	1.0056
1-1/4	0.5137	1.0274
1-3/8	0.5163	1.0326
*1-1/2	0.5239	1.0478

* Surface tension caused the water surface to just touch the launching coil mount.

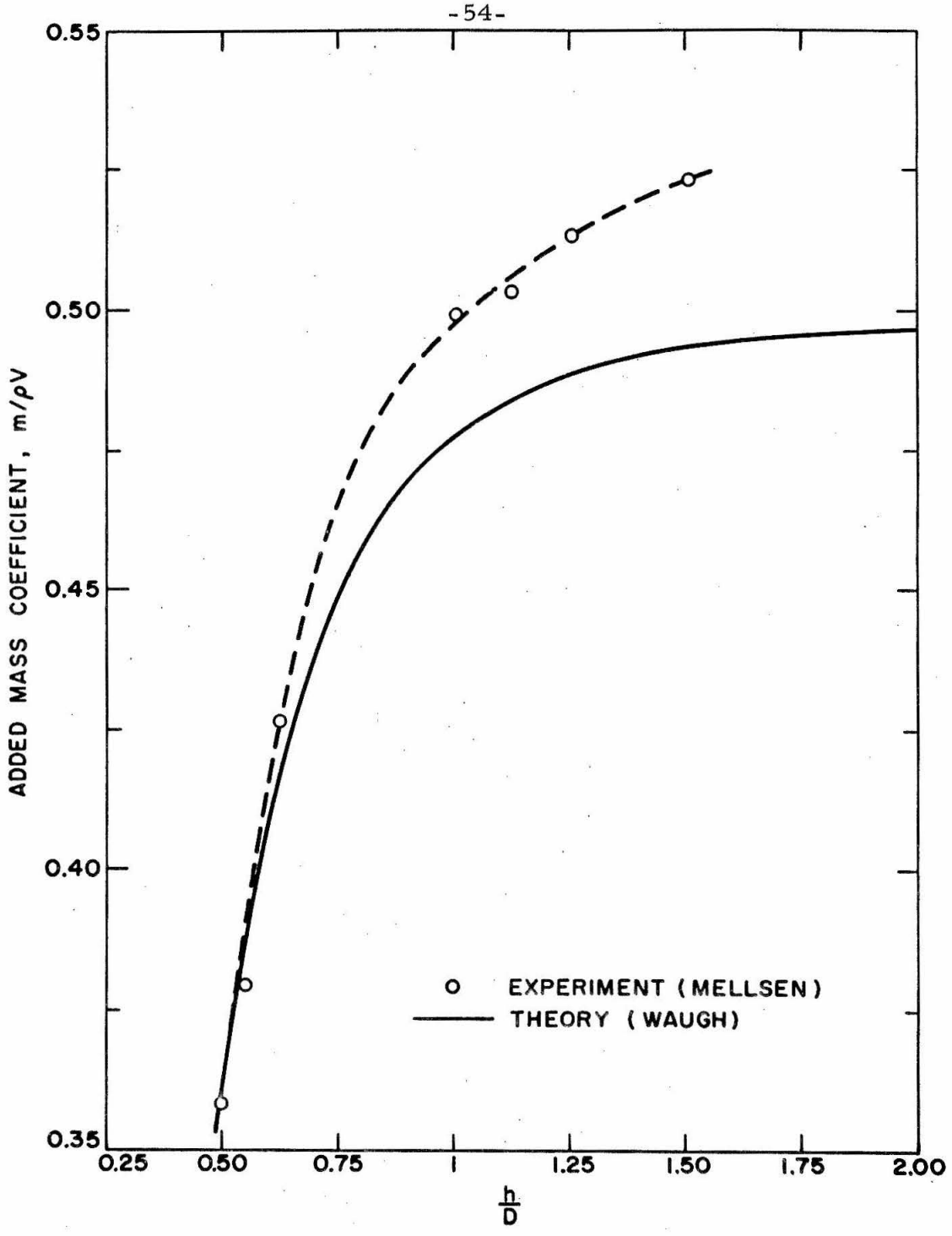

Fig. 7 - Added mass of a sphere accelerated vertically toward a free water surface in a large tank. Depth of sphere center is expressed in diameters.

Table 8

Added Mass of a 1 Inch Diameter Sphere in a 4.45 Inch Diameter Cylinder for Various Depths of the Sphere Below the Free Water Surface in the Cylinder

Initial Depth of Sphere Center h inches	Added Mass Ratio $\frac{m}{\rho V}$	Added Mass at Compared to Added Mass at ∞ $\frac{m_h}{m_\infty}$	Mean Velocity at End of Pulse U_w in. sec.$^{-1}$	Froude No. $\frac{U_w}{\sqrt{gh}}$
1	0.5239	1.0139	56.24	2.89
1-1/4	0.5559	1.0780	53.64*	2.44
1-1/2	0.5508	1.0659	55.31	2.29
2	0.5491	1.0648	53.87*	1.94
3	0.5477	1.0621	54.42	1.60
5	0.5384	1.0440	55.74	1.31
10	0.5403	1.0477	54.90	0.88
19	0.5386	1.0444	55.73	0.67

*Experimental points done at a later date than the remainder of the points. A corresponding set of tests in air was also done for determining the added mass.

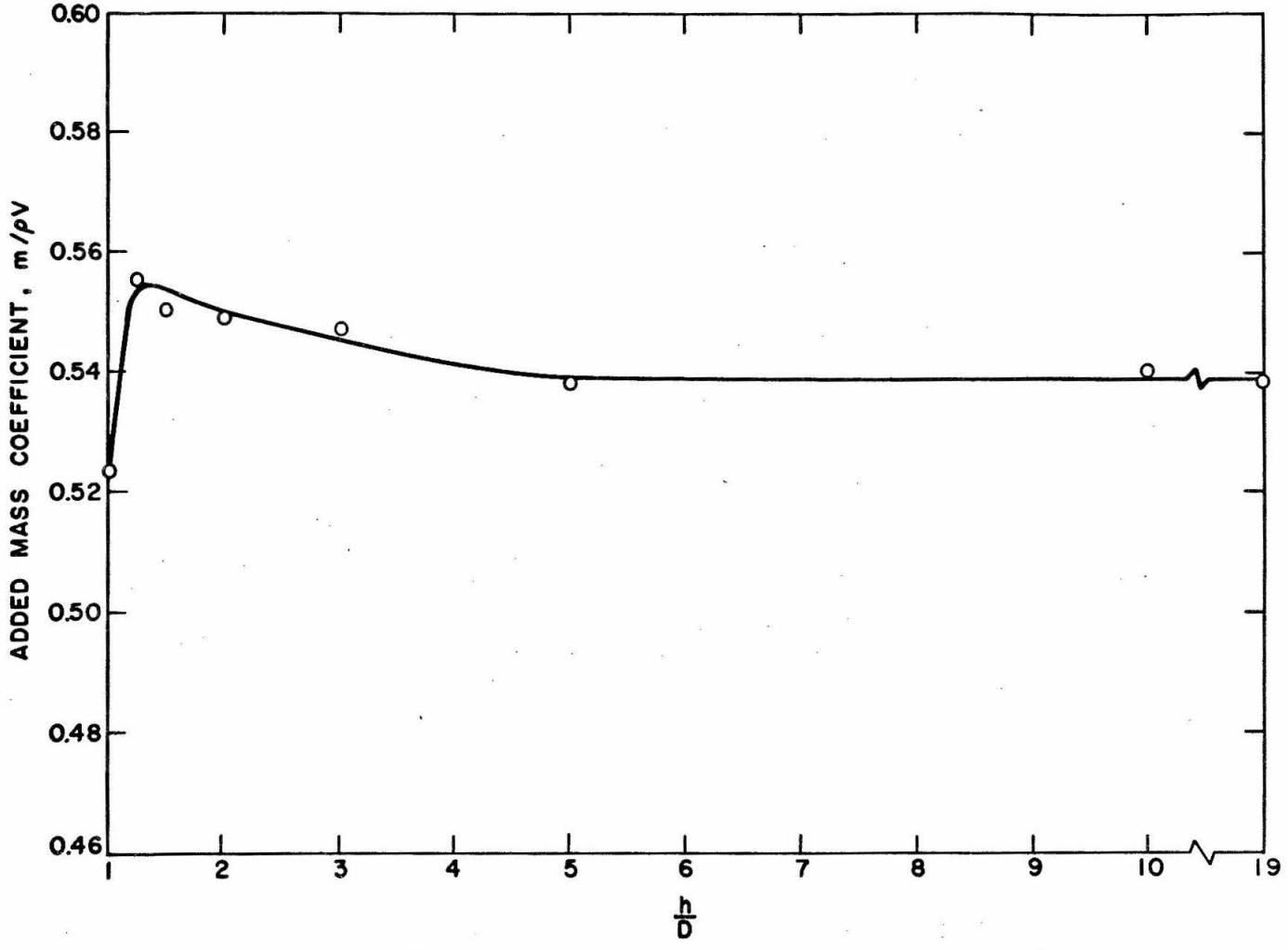

Fig. 8 - Added mass of a 1.004 inch diameter sphere accelerated vertically along the axis of a 4.45 inch I.D. cylinder toward a free water surface. Depth of sphere center is expressed in diameters.

IV. EXPERIMENTAL AND THEORETICAL EVALUATION OF THE REAL FLUID EFFECTS

A. Experimental Data

The fluid used in the experimental tests was No. 7 white mineral oil of density 0.8806 gm. cm. $^{-3}$ and viscosity 63.61 ± 0.10 centipoises at 21°C, measured with a Hoeppler Precision Viscometer. The apparatus and techniques used for obtaining the experimental data were the same as for the tests in water previously described in Section III. The one inch diameter hollow steel sphere was pulsed vertically upward from rest along the axis of the 4.45 inch I.D. lucite cylinder filled with the No. 7 mineral oil so that initially the top surface of the oil and the bottom of the cylinder were both about 20 inches from the center of the sphere. The tests were run at the temperature at which the viscosity of the oil was measured.

Eight individual runs were made to obtain the required experimental data. The following results were obtained.

Table 9

One Inch Diameter Sphere in No. 7 Oil in 4.45" I.D. Cylinder

Test No.	U_∞ in. sec.$^{-1}$	b in. sec.$^{-1}$ int.$^{-1}$	Rise Time to Max. Coil Current	Pulse Duration T/2
550	51.75	-0.418	1.6778×10^{-3} sec.	4.0324×10^{-3} sec.
551	51.60	-0.436	1.6668	4.0292
552	51.92	-0.503	1.6286	4.0274
553	51.85	-0.482	1.6211	4.0260
554	51.90	-0.475	1.6683	4.0285
555	51.41	-0.459	1.6688	4.0240
556	51.89	-0.423	1.6541	4.0295
557	52.01	-0.439	1.6817	4.0312
Mean	51.792	-0.454	1.658×10^{-3}	4.029

U_∞ - final velocity of sphere at end of force pulse

b - mean slope of velocity versus time curve over the first 9 time intervals after the pulse in units of inches per second per interval. The interval used here is one-half millisecond, the time between dots on the photographic data.

For the purpose of calculating added mass a similar set of tests was conducted using air as the fluid medium. The following table of results was obtained.

Table 10

Test No.	U_∞ in. sec.$^{-1}$	Rise Time to Max. Coil Current	Pulse Duration T/2
558	81.04	1.7541×10^{-3} sec.	4.0131×10^{-3} sec.
559	80.52	1.7214	4.0207
560	79.89	1.7341	4.0161
561	79.63	1.7320	4.0254
562	79.39	1.7361	4.0143
563	79.78	1.7234	4.0256
564	79.15	1.6992	4.0087
565	79.52	1.7037	4.0177
Mean Value	79.865	1.726×10^{-3} sec.	4.018

B. The Force Function Used for Accelerating the Sphere

The method of propelling the sphere through the fluid was by the electromagnetic propulsion system described in Section III. B. 4. The axial electromagnetic force as a function of time is given by Eq. 10.

$$F \approx \frac{Kze^{-2\alpha t}\sin^2 \omega t}{(c^2 + z^2)^4} \qquad \text{(Eq. 10)}$$

To use Eq. 10 to obtain the magnetic force as a function of time it was necessary to determine experimentally the circuit parameters α and ω. This was done as follows.

The current flowing in the electromagnetic coil was

$$I = I_o e^{-\alpha t}\sin \omega t \qquad \text{(Eq. 9)}$$

This current was allowed to pass in one direction only by a thyraton. Thus the coil current is cut off at half the period of the circuit,

$$\text{i.e., } \frac{\omega T}{2} = \pi \qquad \text{(Eq. 24)}$$

Table 9 gives the pulse duration measured from the oscilloscope trace of current versus time. Using Eq. 24 and the mean value of T/2 for the eight trials gives

$$\omega = 7.798 \times 10^2 \text{ rad. sec.}^{-1}$$

The maximum current flowing in the propulsion coil is given when

$$\frac{dI}{dt} = 0$$

from which

$$\tan \omega t_{max} = \frac{\omega}{\alpha} \qquad \text{(Eq. 25)}$$

Table 9 gives the rise time to maximum current measured again from the oscilloscope trace previously mentioned. Using the mean value of t_{max} from this in Eq. 25 gives

$$\alpha = 1.944 \times 10^{2} \text{ rad. sec.}^{-1}$$

Equation 10 can be written

$$F \approx Kz(t)e^{-2\alpha t}\sin^2 \omega t \qquad \text{(Eq. 10)}$$

where

$$z(t) = \frac{z}{(c^2 + z^2)^4}$$

The initial value of $z = 2.30$ inches and the radius of the coil, $c = 3.03$ inches.

The sphere moved approximately 1/8 inch while the force pulse acted. Thus z(t) can be considered approximately constant during this time interval and the force function can be written

$$F \approx Ke^{-2\alpha t}\sin^2 \omega t \qquad \text{(Eq. 26)}$$

where K is a constant of proportionality.

A graph of displacement of the sphere as a function of time during the force pulse interval is shown in Fig. 20A of Appendix 4.

C. The Viscous Wall Shear Force

The fundamental boundary layer equations are

$$\frac{\partial u}{\partial t} + u\frac{\partial u}{\partial x} + v\frac{\partial u}{\partial y} = -\frac{1}{\rho}\frac{\partial p}{\partial x} + \nu\frac{\partial^2 u}{\partial y^2}$$

$$\frac{\partial (ur)}{\partial x} + \frac{\partial (vr)}{\partial y} = 0$$

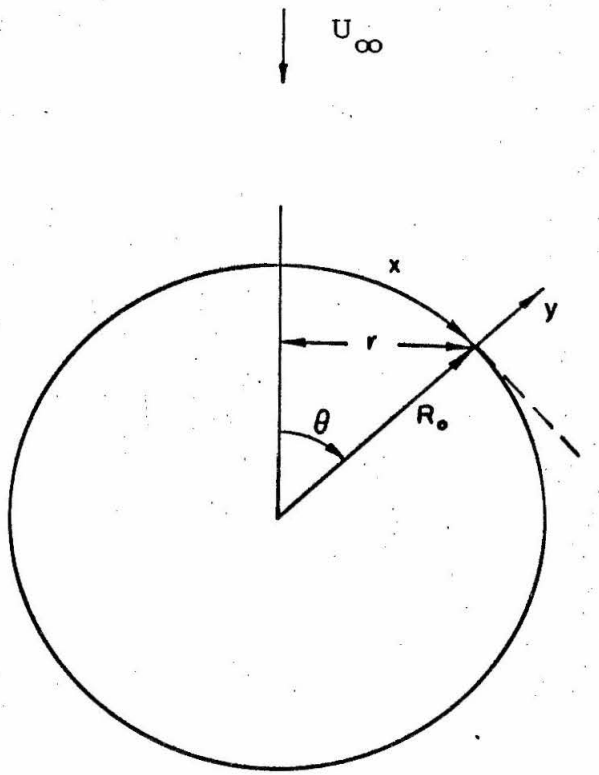

Co-ordinates

The wall shear stress on a sphere launched suddenly from rest at velocity U_∞ at time $t = 0$ is given from the solution of these equations, i.e.,

$$\sigma_{xy} = \mu\left(\frac{\partial u}{\partial y}\right)_{y=0} = \frac{\mu U}{2\sqrt{\nu t}}\left\{\zeta_o''(0) + t\left[\frac{dU}{dx}\zeta_{1a}''(0) + \frac{U}{r}\frac{dr}{dx}\zeta_{1b}''(0)\right] + t^2\left[\left(\frac{dU}{dx}\right)^2\zeta_{2a}''(0) + \frac{Ud^2U}{dx^2}\zeta_{2b}''(0) + \frac{U}{r}\frac{dU}{dx}\frac{dr}{dx}\zeta_{2c}''(0) + \frac{U^2}{r}\frac{d^2r}{dx}\zeta_{2d}''(0) + \frac{U^2}{r^2}\left(\frac{dr}{dx}\right)^2\zeta_{2e}''(0)\right] + \ldots\right\} \qquad \text{(Eq. 27)}$$

where x and y are the coordinates along the surface and perpendicular to the surface respectively.

U = potential flow velocity at the surface of the sphere

u = velocity of the viscous fluid around the sphere

r = perpendicular distance from the axis to the surface of the sphere

μ = dynamic viscosity of the fluid

ν = kinematic viscosity of the fluid

$\zeta_{a\beta}''(0)$ = the numerical coefficients of the series solution to the boundary layer equations evaluated by E. Boltze in his Goettingen thesis (8).

For the motion studied in the experiment it can be shown that the first term makes the largest contribution to the viscous drag and viscous drag impulse. The drag due to the second term integrates to zero due to the fore and aft symmetry of the sphere

and the third term makes a contribution which is only about 0.2 percent of the first term. The detailed calculations are shown in Appendix 1.

The first term corresponds to the exact solution for a plate at zero incidence (10). Since the higher order terms are negligible in comparison with first order terms, a very good approximation of the viscous wall drag can be found by considering only this term.

The solution to the problem of the sliding flat plate is shown in Ref. 9. The problem and its solution are briefly stated here for convenience.

Let the fluid occupy the region $y > 0$ and let the x axis coincide with the flat plate. Furthermore, assume that for $t < 0$ the fluid is at rest, $u = 0$ and the pressure $p = p_\infty$. At $t = 0$ the flat plate starts moving parallel to itself with velocity $f(t)$. It is easily seen that the fluid velocity perpendicular to the plate, v, remains zero and the pressure p remains constant so that the Navier Stokes equations reduce to

$$u_t = \nu u_{yy} \qquad \text{(Eq. 28a)}$$

$$\Omega_t = \Omega_{yy} \qquad \text{(Eq. 28b)}$$

$$\Omega = -u_y \qquad \text{(Eq. 28c)}$$

where Ω is the vorticity and u is the fluid velocity parallel to and past the plate. In this case both velocity and vorticity obey the simplest form of the heat equation.

The fundamental solution of the heat equation $\frac{\partial T}{\partial t} = K\frac{\partial^2 T}{\partial x^2}$ is

$$\frac{e^{-\frac{x^2}{4kt}}}{2\sqrt{\pi kt}}$$

which represents the one-dimensional temperature wave resulting from instantaneously introducing heat of amount ρc at the point $x = 0$ at $t = 0$ (ρ = density, c = specific heat). The negative x derivative of the fundamental solution is called an instantaneous dipole or doublet.

It is known from the theory of the heat equation that the solution may be obtained by a doublet distribution along the plate of strength $f(t)$ per unit length. Thus

$$u(y, t) = \int_0^t \frac{f(\tau) y\, e^{-\frac{y^2}{4\nu(t-\tau)}} d\tau}{2\sqrt{\pi\nu\,(t-\tau)^3}} \qquad \text{(Eq. 29)}$$

The vorticity may be found directly as follows. On the plate its normal derivative

$$\frac{\partial \Omega}{\partial y} = -\frac{\partial^2 u}{\partial y^2}$$

is prescribed to be

$$-\frac{1}{\nu}\frac{df}{dt} .$$

The resulting vorticity wave may then be found by a distribution of source strength along the plate equal to twice the normal derivative of Ω. This gives

$$\Omega = \int_0^t \frac{f'(\tau)e^{-\frac{y^2}{4\nu(t-\tau)}}d\tau}{\sqrt{\pi\nu(t-\tau)}} + \frac{f(0)e^{-\frac{y^2}{4\nu t}}}{\sqrt{\pi\nu t}} \qquad \text{(Eq. 30)}$$

The skin friction at the plate σ_{xy} is directly proportional to Ω:

$$\sigma_{xy} = \mu\left(\frac{\partial u}{\partial y}\right)_{y=0} = -\mu\Omega(0, t) \qquad \text{(Eq. 31)}$$

Now for the problem of the sphere launched in the viscous fluid by the electromagnetic propulsion system, a very close approximation to the viscous shear stress may be found. From Eq. 26

$$f(t) \approx K\int_0^t e^{-2\alpha t}\sin^2\omega t\, dt$$

and

$$f'(t) \approx Ke^{-2\alpha t}\sin^2\omega t \qquad \text{(Eq. 32)}$$

Equation 32 assumes that gravitational force and viscous forces are small in comparison with the magnetic force. The relative magnitudes of these forces are shown later in this discussion.

Substituting Eq. 30 into Eq. 31 gives

$$\sigma_{xy} = \mu\int_0^t \frac{f'(\tau)d\tau}{\sqrt{\pi\nu(t-\tau)}} + \frac{\mu f(0)}{\sqrt{\pi\nu t}} \qquad \text{(Eq. 33)}$$

and substituting Eq. 32 into Eq. 33 gives

$$\sigma_{xy} = \mu K \int_0^t \frac{e^{-2a\tau} \sin^2 \omega\tau \, d\tau}{\sqrt{\pi\nu(t - \tau)}} \qquad \text{(Eq. 34)}$$

The value of K in Eq. 32 can be determined from the results at the end of the force pulse in the experimental tests, where the velocity of the fluid is known:

$$U_\infty(\tfrac{T}{2}) = K \int_0^{T/2} e^{-2a\tau} \sin^2 \omega\tau \, d\tau$$

Then

$$K = \frac{U_\infty(\frac{T}{2})}{\int_0^{T/2} e^{-2a\tau} \sin^2 \omega\tau \, d\tau}$$

Thus the wall shear stress at any time t during the force pulse is given by

$$\sigma_{xy} = \frac{U_\infty(\frac{T}{2}) \rho \sqrt{\frac{\nu}{\pi}} \int_0^t \frac{e^{-2a\tau} \sin^2 \omega\tau \, d\tau}{\sqrt{(t - \tau)}} \quad 0 \le t \le T/2}{\int_0^{T/2} e^{-2a\tau} \sin^2 \omega\tau \, d\tau} \qquad \text{(Eq. 35)}$$

The total impulse due to the shearing stress during the propulsive pulse period is

$$I_{\sigma_{xy}} = \int_0^{T/2} \sigma_{xy}\, dt = \frac{2U_\infty(\frac{T}{2})\rho\sqrt{\frac{\nu}{\pi}} \int_0^{T/2} \sqrt{\frac{T}{2} - \tau}\; e^{-2a\tau} \sin^2\omega\tau\, d\tau}{\int_0^{T/2} e^{-2a\tau} \sin^2\omega\tau\, d\tau}$$

(Eq. 36)

Equations 35 and 36 which give the wall shear stress and the wall shear stress impulse on a flat plate will now be applied for the determination of the wall drag and impulse on a sphere. As has already been shown the wall shear stress is very nearly directly proportional to the velocity outside the boundary layer. Then it is only necessary to know the velocity distribution around the sphere and take this into account in integrating the wall shear stress over the whole sphere to get the total wall shear drag.

D. The Free Stream Velocity

The free stream velocity for flow about a sphere in a circular cylinder can be found by considering the vector potential in Ref. 3. It is only briefly stated here. The details of the calculation are shown in Appendix 2.

The vector potential is

$$A_\phi = A_\phi' + A_\phi'' + A'_\phi{}'' \qquad \text{(Eq. 37)}$$

The velocity of the fluid is given by

$$V = \text{curl } A_\phi \qquad \text{(Eq. 38)}$$

The flow velocity adjacent to the sphere is

$$U(\theta) = U_\infty \sin\theta \left[1 + \frac{C_o}{3} + 0.5312 \left(\frac{R_o}{a}\right)^3 C_o + 0.2001 \left(\frac{R_o}{a}\right)^5 C_o - 1.000 \left(\frac{R_o}{a}\right)^5 \cos^2\theta \, C_o + \ldots \right] \qquad \text{(Eq. 39)}$$

R_o = radius of sphere

a = radius of the cylinder

C_o = constant coefficient depending upon $\frac{R_o}{a}$

For the experimental tests performed in the laboratory

$$\frac{R_o}{a} = 0.2256, \quad C_o = 1.5157$$

giving

$$U(\theta) = U_\infty (1.5146 \sin\theta - 0.0009 \cos^2\theta \sin\theta) \qquad \text{(Eq. 40)}$$

The drag and drag impulse for the sphere launched along the axis of the cylinder are now found using Eqs. 35, 36 and 40. The drag at t = T/2 due to wall shear stress is

$$D = \frac{\rho\sqrt{\frac{\nu}{\pi}} \int_0^\pi 2\pi R_o^2 \sin^2\theta \, U(\theta) \, d\theta \int_0^{T/2} \frac{e^{-2a\tau} \sin^2\omega\tau \, d\tau}{\sqrt{(t-\tau)}}}{\int_0^{T/2} e^{-2a\tau} \sin^2\omega\tau \, d\tau}$$

$$= 0.991 \pm 0.002 \times 10^{4} \text{ gm. in. sec.}^{-2} \qquad \text{(Eq. 41)}$$

The units are mixed for convenience here. In the laboratory the scale used for weighing was calibrated in grams and measurements of distance were done in inches.

The drag impulse due to wall shear stress over the propulsive pulse period is

$$I_D = \frac{2\rho\sqrt{\frac{\nu}{\pi}} \int_0^{\pi} 2\pi R_o^2 \sin^2\theta \, U(\theta) \, d\theta \int_0^{T/2} \sqrt{\frac{T}{2} - \tau} \, e^{-2a\tau} \sin^2\omega\tau \, d\tau}{\int_0^{T/2} e^{-2a\tau} \sin^2\omega\tau \, d\tau}$$

$$= 38.94 \pm 0.07 \text{ gm. in. sec.}^{-2} \qquad \text{(Eq. 42)}$$

For details of the evaluation of D and I_D using Eqs. 41 and 42, see Appendix 3.

For Eqs. 41 and 42 to be valid it is necessary that separation of the boundary layer did not occur. From Page 218 of Ref. 10 the distance travelled before separation starts for a sphere launched impulsively from rest is $S_s = 0.392\ R_o$. The problem at hand was solved with high accuracy by superposition of impulses. The minimum distance that the sphere could travel before separation due to the first of these impulses in absence of the other impulses which followed was $S_s = 0.392\ R_o = 0.197$ inches. From the graph in Fig. 20A of Appendix 4 the total displacement of the sphere during

the force pulse was 0.112 inches, well within the distance given above.

One can also consider separation by looking at the problem in a slightly different way. The motion of the sphere can be compared with the case of uniform acceleration which was solved by H. Blasius (10). From this solution it is seen that separation occurs at a later time and longer distance from the starting point for constant acceleration than for motion started impulsively.

In short, motion started impulsively is the worst case. Then for the problem at hand where the acceleration as a function of time was a damped half sine wave, the sphere travelled a considerable distance after the force pulse was over before separation started.

E. The Evaluation of the Added Mass of a Sphere in a Viscous Fluid

For the sphere launched in the viscous fluid, equating the total impulse acting on the sphere to its momentum change gives

$$\int_0^{T/2} (F_o - D - G_o)\,dt = \int d(M' U_\infty) = \Big[(M + m)U_\infty\Big]_{t=0}^{t=T/2} \qquad \text{(Eq. 43)}$$

where

F_o = magnetic propulsive force

D = viscous drag force due to wall shear stress

G_o = negative buoyancy force

M = mass of the sphere

m = added mass

U_∞ = velocity of sphere through the fluid.

For a sphere launched in air the impulse momentum relationship is

$$\int_0^{T/2} (F_a - G_a)\, dt = MU_a \qquad \text{(Eq. 44)}$$

where

F_a = magnetic propulsive force in air

G_a = gravitation force on the sphere.

Defining the impulses by

$$I_a = \int_0^t F_a dt$$

and using Eqs. 43 and 44, the following relationship can be deduced.

$$\frac{m}{M} = \frac{1}{U_\infty}\left[\frac{U_a + \frac{I_{G_a}}{M}}{\left(\frac{I_{F_a}}{I_{F_o}}\right)} - \frac{I_D}{M} - \frac{I_{G_o}}{M}\right] - 1 \qquad \text{(Eq. 45)}$$

Here $\frac{I_{F_a}}{I_{F_o}}$ is found using Eq. 23 and Table 3. The displacement S' was 0.1010 inches giving $\frac{I_{F_a}}{I_{F_o}} = 1.0093$.

Using the values of U_a and U_∞ from Table 9, I_D from

Eq. 42, and the values of remaining terms on the R.H.S.,

$$\frac{m}{M} = \frac{1}{51.79}\left(\frac{79.87 + 1.51}{1.0093} - 4.186 - 0.268\right) - 1$$

$$= 0.4709 \pm 0.0061 \qquad \text{(Eq. 46)}$$

The details of the calculation of the error are shown in Appendix 3.

The relative magnitudes of the various force impulses acting on the sphere can be seen by examining the numbers in Eq. 46 and comparing them with their counterparts in Eq. 45. The order of the appearance of the terms in these equations is preserved for this purpose.

The added mass for a one-inch diameter sphere in a 4.45 inch diameter cylinder using an ideal fluid is found from potential theory to be (based on Ref. 7):

$$\frac{m}{\rho V} = 0.5157 \qquad \text{(Eq. 47)}$$

where ρ is the density of the fluid, V is the volume of the fluid displaced by the sphere, and m is the added mass.

When the sphere moves in a viscous fluid its boundary layer grows. Thus the moving body inside the potential flow increases in size. This in turn causes the added mass of this body to increase. Assuming that the sphere plus its boundary layer is still a sphere, the added mass ratio becomes

$$\frac{m}{\rho V + M_D} = 0.5157 \qquad \text{(Eq. 48)}$$

where M_D is the mass of fluid carried along in the boundary layer of the sphere due to shear force in the fluid.

The quantity M_D can be determined by considering the drag impulse from Eq. 42. Equating the drag impulse I_D to its corresponding momentum change, we have

$$I_D = \int_0^{T/2} D\,dt = \int_0^{T/2} d(M_D U)$$

or

$$I_D = M_D U_\infty \Big|_0^{T/2} = M_D(\tfrac{T}{2})U(\tfrac{T}{2}),$$

the momentum of fluid carried along with the sphere. Since the drag impulse I_D can be found from Eq. 42 and the velocity of the sphere U_∞ is known at the end of the force pulse, the mass M_D can be found.

$$M_D = \frac{I_D}{U_\infty(\frac{T}{2})} = \frac{38.94 \pm 0.07 \text{ gm. in. sec.}^{-1}}{51.79 \pm 0.07 \text{ in. sec.}^{-1}}$$

$$= 0.7519 \pm 0.0024 \text{ gm.}$$

so that

$$\rho V + M_D = 7.6988 \pm 0.0017 \text{ gm.} + 0.7159 \pm 0.0024 \text{ gm.}$$

$$= 8.4507 \pm 0.0041 \text{ gm.}$$

Then

$$\frac{M}{\rho V + M_D} = \frac{9.3035 \pm 0.0001 \text{ gm.}}{8.4507 \text{ gm.}} = 1.1009 \pm 0.0005 .$$

Thus, using Eqs. 46 and 48

$$\frac{m}{\rho V + M_D} = \left(\frac{m}{M}\right)\left(\frac{M}{\rho V + M_D}\right) = 0.5184 \pm 1.4\%$$

Here the possible error in the impulse correction has not been accounted for. Since the total correction is less than 3 percent of the added mass coefficient allowing a generous error of 15 percent in the correction would still keep the total experimental error under ±2 percent.

Comparison of the experimentally evaluated added mass to its corresponding theoretical value gives:

$$\frac{m_{\text{experimental}}}{m_{\text{theoretical}}} = 1.0052 ,$$

a very close agreement, well within the estimated total experimental error.

F. Comparison of the Viscous Drag Evaluated from Boundary Layer Theory to Viscous Drag Evaluated Directly from Experiment

After the propulsive force pulse was over the sphere was allowed to coast in the fluid and its motion was observed. A velocity versus time curve for this motion is shown in Fig. 10. A similar curve for the corresponding tests in air is shown in Fig. 9. The points plotted are the mean values of eight runs. The deviation of

the points from the smooth curve through them are not only due to statistical deviations but for the most part, they are due to systematic fluctuations of the motion. Examination of the data showed that the velocity at a specific time in each test separately indicated that the velocity deviated uniformly for all eight tests. From Page 218, Ref. 10, for a sphere launched impulsively from rest separation of the boundary layer is calculated to take place after the sphere has travelled 0.392 R where R is the sphere radius. This point corresponds to the time, 1-1/2 milliseconds, after the propulsive pulse is over. Large deviation of the points from the smooth curve in Fig. 10 appears to begin about this time.

To determine the slope of the velocity-time curve at time $t_c = 0$, where t_c is the time elapsed after the propulsive force is over, corresponding to the end of the force pulse, various methods were employed. The tangent to the curve at $t_c = 0$ drawn by eye gave a slope of 1.250×10^3 in. sec.$^{-2}$. A straight line fitted by the method of least squares through the first four points, i.e., between $t_c = 0$ and t_c = 1-1/2 m.s., on each test gave a mean slope of 1.380×10^3 in. sec.$^{-2}$ for eight tests. Fitting a parabola by least squares through the mean value of each point for all points from $t_c = 0$ to t_c = 9-1/2 milliseconds, i.e., all the points on the graph in Fig. 10, gives an initial slope of 1.032×10^3 in. sec.$^{-2}$.

The slope of the velocity curve can also be found by considering the forces acting on the sphere. Equating force to its corresponding momentum change gives

$$F = \frac{d(M'' u)}{dt}$$

or

$$- D - (M - \rho V)g = M'' \frac{du}{dt} + u \frac{d}{dt} (m + M_D)$$

where

$$M'' = m + M_D + M$$

so

$$\frac{du}{dt} = \frac{-D - (M - \rho V)g - u \frac{dm}{dt} + u \frac{dM_D}{dt}}{M + M_D + m}$$

Now, from Eq. 48,

$$m = 0.5157 (\rho V + M_D), \quad M_D(t) = \frac{M_D(\frac{T}{2})\sqrt{t}}{\sqrt{\frac{T}{2}}}$$

so

$$\left[\frac{dm}{dt}\right]_{t = T/2} = \frac{0.5157 \, M_D(\frac{T}{2})}{T}$$

also

$$\left[\frac{dM_D}{dt}\right]_{t = T/2} = \frac{M_D(\frac{T}{2})}{T}$$

$$\frac{d}{dt}(m + M_D) = 141.5 \text{ gm. sec.}^{-1}, \quad (M - \rho V)g = 6.19 \times 10^2 \text{ in. sec.}^{-2},$$

$$\frac{du}{dt} = \frac{-(0.9910 \times 10^4 - 0.062 \times 10^4)\text{gm. in. sec.}^{-2}}{9.3035 \text{ gm.} + 0.7519 \text{ gm.}}$$

$$\frac{-(51.79)\text{in. sec.}^{-1}(148.3)\text{gm. sec.}}{+ 0.5157 \, (0.7519 + 7.6988)\text{gm.}} = -1.239 \times 10^3 \text{ in. sec.}^{-2}$$

This value of $\frac{du}{dt}$ agrees favorably with the slope of the curve evaluated by examining the motion directly.

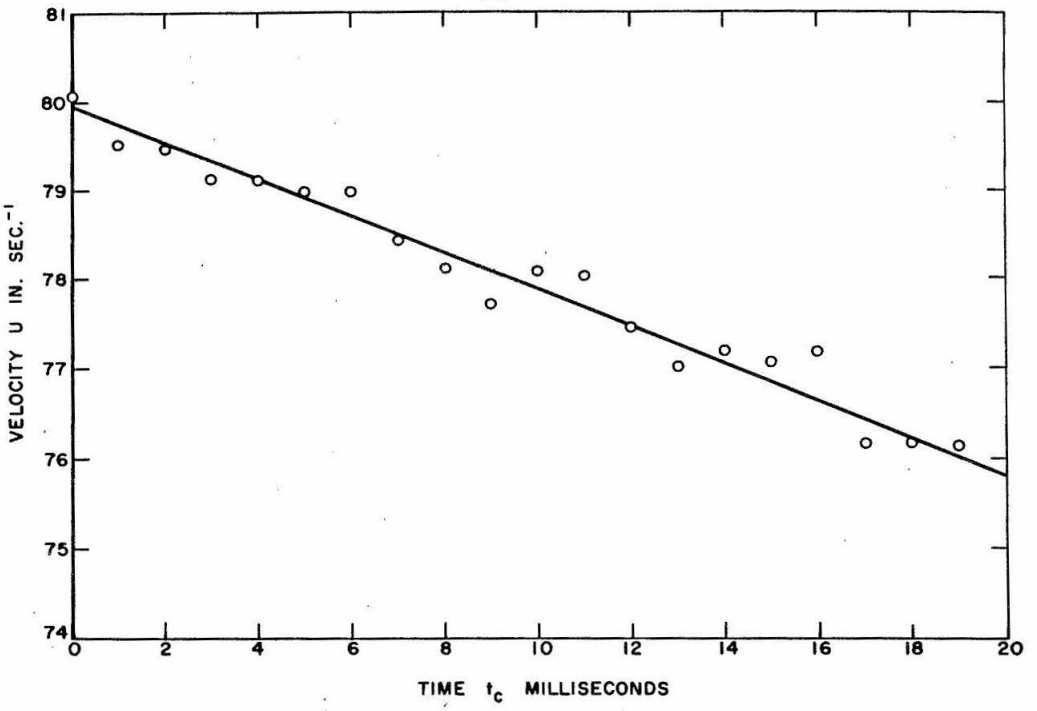

Fig. 9 - Sphere in air

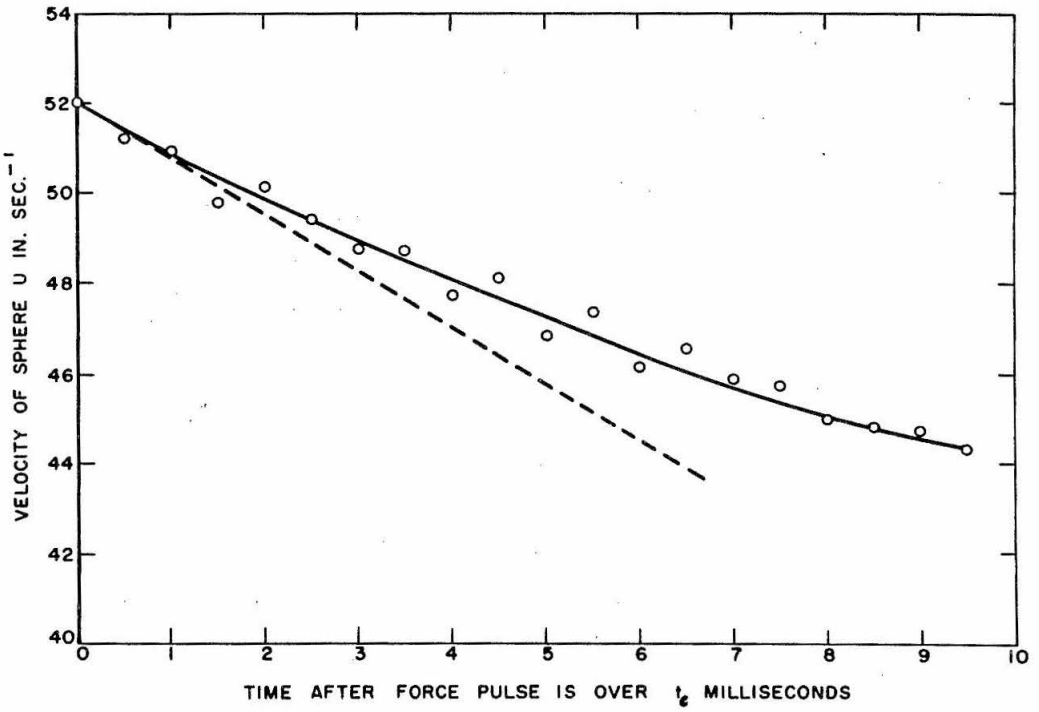

Fig. 10 - Sphere in No. 7 mineral oil in 4.45 inch I.D. cylinder

Figs. 9 and 10 - Vertical upward velocity of 1.004 inch diameter sphere after propulsive force ended

V. CORRECTION FOR REAL FLUID EFFECTS IN THE TESTS IN WATER

The method used for evaluating real fluid effects in the previous section is applied to the tests in water. The potential flow velocity at the surface of the sphere is given as in the previous section by

$$U(\theta) = \left[1 + \frac{C_o}{3} + 0.5312 \left(\frac{R_o}{a}\right)^3 C_o + 0.2001 \left(\frac{R_o}{a}\right)^5 C_o \right] U_\infty \sin\theta$$

$$- 1.000 \left(\frac{R_o}{a}\right)^5 C_o U_\infty \sin\theta \cos^2\theta \qquad \text{(Eq. 39)}$$

From this is obtained the free stream velocity required for calculating viscous drag.

Table 11

Velocity Distribution for Flow Around a Sphere in a Circular Cylinder

Cylinder I.D. (Inches)	Coefficient C_o	Free Stream Velocity at the Surface of the Sphere $U(\theta)$
4.450	1.5157	$(1.515 \sin\theta - 0.0009 \sin\theta \cos^2\theta)\, U_\infty$
3.480	1.5302	$(1.531 \sin\theta - 0.0030 \sin\theta \cos^2\theta)\, U_\infty$
2.459	1.5883	$(1.591 \sin\theta - 0.0180 \sin\theta \cos^2\theta)\, U_\infty$
1.940	1.6924	$(1.701 \sin\theta - 0.0632 \sin\theta \cos^2\theta)\, U_\infty$
1.718	1.7907	$(1.811 \sin\theta - 0.1230 \sin\theta \cos^2\theta)\, U_\infty$
1.477	2.0172	$(2.037 \sin\theta - 0.292 \sin\theta \cos^2\theta)\, U_\infty$
1.236	2.7177	$(2.798 \sin\theta - 0.960 \sin\theta \cos^2\theta)\, U_\infty$
1.109	3.9388	$(4.320 \sin\theta - 2.386 \sin\theta \cos^2\theta)\, U_\infty$

The impulse due to viscous drag can now be found using Eq. 42. For the tests in water

$$\nu = 1.007 \times 10^{-2} \text{ cm. sec.}^{-1}$$
$$\rho = 0.9982 \text{ gm. cm.}^{-3} \qquad \text{at } 21^{\circ}\text{C}$$

$U_{\infty}(\frac{T}{2}) = U_w$, from Table 4.

Then using Eq. 45 the value of $\frac{m}{M}$ can be found and hence $\frac{m}{\rho V}$. The following table gives the results.

Table 12

Added Mass Corrected for Impulse Due to Viscous Drag

Cyl. I.D. 2a (In.)	Drag Impulse $\frac{I_D}{M}$ ($\frac{\text{in.}}{\text{sec.}}$)	Added Mass $\frac{m_{ex}}{\rho V}$	Ratio $\frac{m_{th}}{\rho V}$	Comparison of Exp. to Theory $\frac{m_{ex}}{m_{th}}$
4.450	0.6383 ± 0.0001	0.5128	0.5157	0.9944
3.480	0.6347	0.5376	0.5302	1.0140
2.459	0.6398	0.5816	0.5883	0.9886
1.940	0.6366	0.6947	0.6924	1.0033
1.718	0.6369	0.7907	0.7907	1.0075
1.477	0.6350	1.0172	1.0172	0.9818
1.236	0.6153 + 0.0008*	1.7177	1.7177	1.0098
1.101	0.5895	-	-	-
Mean for 7 largest cylinders				0.9999

* See Appendix 2 for details of calculation.

Table 13

Added Mass Corrected for Impulse Due to Viscous Drag
and Boundary Layer Displacement Effect

Cyl. I.D.	ρV(gm.)	M_D(gm.)	$\rho V + M_D$ (gm.)	$\frac{m}{\rho V + M_D}$	$\frac{m_{ex}}{m_{th}}$
4.450	8.6182	0.1066	8.7248	0.5094	0.9878
3.480	8.6182	0.1157	8.7339	0.5334	1.0060
2.459	8.6186	0.1116	8.7302	0.5776	0.9818
1.940	8.6184	0.1188	8.7372	0.6892	0.9954
1.718	8.6184	0.1257	8.7741	0.7897	0.9987
1.477	8.6184	0.1392	8.7576	0.9885	0.9718
1.236	8.6186	0.1833	8.8019	1.7084	0.9946
1.101	8.6185	-	-	-	-
Mean for 7 largest cylinders					0.9909

VI. SUMMARY AND CONCLUSIONS

The method used for evaluating the real fluid effects on added mass gave very good agreement between experiment and theory. Neglecting the effect of the boundary layer on the potential flow around the sphere and its boundary layer, or in other words, considering only the effect of wall shear stress on the resistance to motion, the experimentally evaluated added mass for the tests in oil would be

$$\frac{m}{\rho V} = 0.5690$$

The corresponding ratio of experimental to theoretical added mass is

$$\frac{m_{ex}}{m_{th}} = \frac{0.5690}{0.5157} = 1.1033$$

To evaluate the effect of the boundary layer around the sphere on the free stream flow two steps were taken.

(1) The sphere plus its boundary layer was assumed to be still a sphere. Then since it is known that added mass in a potential flow is independent of the history of the flow, one can conclude that the theoretical added mass ratio in the free stream flow was unchanged. Thus for the largest test cylinder for which the wall effect remained effectively unchanged by the boundary layer

$$\frac{m}{\rho V + M_D} = 0.5157$$

(2) The size of the sphere plus its boundary layer at the end of the propulsive force interval was determined by the momentum deficiency caused by the wall shear stress. The velocity of the sphere at the end of the force pulse was measured and the impulse due to the wall shear stress was calculated using boundary layer theory. From these quantities the mass deficiency was calculated by the relationship

$$I_D = M_D U_\infty \int_0^{T/2}$$

Using these ideas the ratio of experimental to theoretical added mass for the tests in oil was

$$\frac{m_{ex}}{m_{th}} = \frac{0.5184}{0.5157} = 1.0052$$

which is well within the experimental error which was estimated to be less than 2 percent.

The same method was then applied to the tests in water where the dynamic viscosity was about 1/64th of that of the oil. The mean correction for real fluid effects on the tests in the seven largest cylinders was 2.83 percent of the theoretical added mass, giving for these cylinders a mean ratio of experimental to theoretical added mass of

$$\frac{m_{ex}}{m_{th}} = 0.9902\%$$

The results of the investigation show that the methods used gave very good agreement between the experiments and corresponding theory.

An interesting observation was made in the free surface tests. The added mass as a function of initial depth was found to have a maximum for an initial depth of the sphere center, h, in the neighborhood of 1-1/4 inches. At maximum added mass the Froude number based on the velocity of the sphere at the end of the propulsive force was 2.2. The added mass at the maximum was about 3 percent above its deep water value, and added mass decreased very rapidly from the depth of the maximum to smaller values of the depth h.

The experimentally evaluated added mass of the sphere in the seven largest cylinders showed uniformly close agreement with theory; however, the experimentally evaluated added mass in the smallest cylinder was distinctly higher than its corresponding theoretical value. The radius ratio here was $\frac{R_o}{a} = 0.9053$. At this value of $\frac{R_o}{a}$ the slope of the added mass versus radius ratio curve is very high and the added mass is very sensitive to changes in effective sphere radius due to boundary layer growth. The interaction of the boundary layer around the sphere with the cylinder wall is very complicated and no quantitative evaluation of its effect on the added mass was made. However, qualitatively, it can easily be seen that the effect of the

presence of a boundary layer is to increase the effective added mass of the sphere. The boundary layer presence causes a greater constriction through which the potential flow must pass, thereby causing an increase in effective added mass. A smaller counteracting effect in the boundary layer is due to the high velocity of the fluid through the constriction between the sphere and the cylinder. The boundary layer thickness at the greatest constriction is kept thin by the high velocity of the flow through this region. To get some feel for the magnitude of the distances involved a calculation was made of mean boundary layer thickness at the end of the force pulse. The calculation based on the momentum deficiency due to wall shear stress gave

$$M_D = \left(\frac{I_D}{M}\right)\frac{M}{U_\infty} = 0.2688 \text{ gm.}$$

giving

$$\delta_M \approx \frac{M_D}{\rho 4\pi R^2} = 0.005 \text{ inches.}$$

This gave

$$\frac{R_o + \delta_M}{a} = \frac{2(0.502 + 0.005)}{1.109} = 1.03$$

i.e., the mean boundary layer momentum thickness plus the sphere radius is actually larger than the radius of the cylinder.

The shapes of the mean velocity versus time curves in Figs. 10A to 17A indicate strong interaction of the boundary layers with the cylinder walls in the two smallest cylinders. These curves represent

the velocity of the sphere as a function of time beginning at the end of the propulsive force pulse. For the six largest cylinders these lines are very nearly straight; however, for the second smallest cylinder the curve shows a slight increase in negative slope with increasing time, and for the smallest cylinder this increase is very marked. This implies that there was a force increasing with time acting to decelerate the sphere. The force might have been caused by the growing boundary layer contacting both the sphere and the cylinder wall which produced an increasing shear force to act on the sphere. Another possible cause might have been the contracting of the space between the sphere and the wall caused by the growing boundary layer, which produced a strong increase in the effective added mass due to the high velocity required to get the fluid past the sphere.

In evaluating the velocity of the sphere, U_w, in the smallest cylinder it was necessary to fit a shorter straight line to the "coasting" displacement-time data. Here it was found that using only six displacement-time points gave a reasonably good straight line. In other words, the velocity of the sphere during the first 2-1/2 milliseconds after the force pulse ended was approximately linear for the purpose of determining the velocity U_w. For all the other cylinders at least ten points were used in each velocity-time line. The straightness of the lines was checked by fitting more points and comparing the slope and intercept giving U_w, to the slope and intercept of the shorter lines. It was found that accurate results could be achieved using these straight lines fitted by the method of least squares.

REFERENCES

1. Lamb, Sir Horace, "Hydrodynamics", 6th Edition, Cambridge University Press, 1959, pp. 123-124.
2. Birkhoff, G., "Hydrodynamics", Princeton University Press, 1960, Chapter 6.
3. Smythe, W. R., "Flow Around a Spheroid in a Circular Tube", J. of The Physics of Fluids, May 1964.
4. Waugh, J. G. and Ellis, A. T., "The Variable-Atmosphere Wave Tank", Cavitation Research Facilities and Techniques, A.S.M.E., 1964.
5. Smythe, W. R., "Static and Dynamic Electricity", 2nd Edition, McGraw Hill, 1950.
6. Waugh, J. G., Ellis, A. T., and Mellsen, S. B., "Techniques for Metric Photography", J. of The Society of Motion Picture and Television Engineers, Vol. 75, No. 1, January 1966.
7. Tippet, L. H. C., "The Methods of Statistics", 3rd Edition, Williams and Norgate Ltd., 1945.
8. Boltze, E., "Grenzschichten an Rotationskorpen in Flussigkeiten mit kleiner Reibung", Dissertation, Gottingen, 1908.
9. Moore, F. K., "Theory of Laminar Flows", Princeton University Press, 1964.

10. Schlichting, H., "Boundary Layer Theory", 4th Edition, McGraw Hill, 1960.

11. Page, L., and Adams, N. I., "Principles of Electricity", Van Nostrand, 1936.

12. Wayland, H., "Differential Equations Applied in Science and Engineering", Van Nostrand, 1959.

13. Hodgman, C. D., Weast, R. C., and Wallace, C. W., "Handbook of Chemistry and Physics", 35th Edition, Chemical Rubber Publishing Co., Cleveland, Ohio, 1953-54.

APPENDIX 1

Details of the Calculation of Wall Shear Drag Using Boltze's Solution

The wall shear stress on a sphere is given by:

$$\sigma_{xy} = \frac{\mu U}{2\sqrt{\nu t}}\left\{\zeta_o''(0) + t\left[\frac{dU}{dx}\zeta_{1a}''(0) + \frac{U}{r}\frac{dr}{dx}\zeta_{1b}''(0)\right]\right.$$

$$+ t^2\left[\left(\frac{dU}{dx}\right)^2\zeta_{2a}''(0) + U\frac{d^2U}{dx^2}\zeta_{2b}''(0) + \frac{U}{r}\frac{dU}{dx}\frac{dr}{dx}\zeta_{2c}''(0)\right.$$

$$\left.\left. + \frac{U^2}{r}\frac{d^2r}{dx^2}\zeta_{2d}''(0) + \frac{U^2}{r^2}\left(\frac{dr}{dx}\right)^2\zeta_{2e}''(0)\right]\right\} \qquad \text{(Eq. 27)}$$

where

$$\theta = \frac{x}{R_o}, \quad r(x) = R_o \sin\frac{x}{R_o}, \text{ and } U = \frac{3}{2}U_\infty \sin\frac{x}{R_o}$$

for a sphere in an infinite fluid.

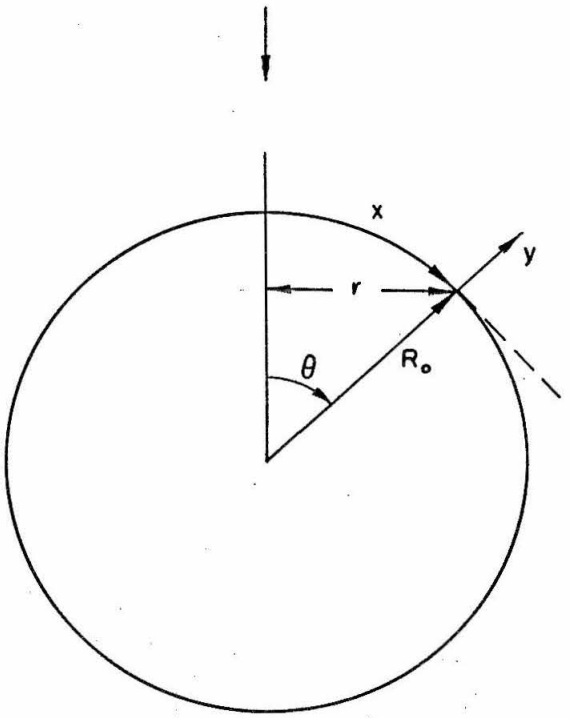

Fig. 1A - Co-ordinates

The derivatives in Eq. 27 for a sphere in an infinite fluid are then given as follows.

$$\frac{dU}{dx} = \frac{3U_\infty \sin\phi}{2R_o}, \quad \left(\frac{dU}{dx}\right)^2 = \frac{9}{4}\frac{U_\infty^2 \cos^2\phi}{R_o^2}$$

$$\frac{d^2U}{dx^2} = -\frac{3}{2}\frac{U_\infty \sin\phi}{R_o^2}, \quad U\frac{d^2U}{dx^2} = -\frac{9}{4}\frac{U_\infty^2 \sin^2\phi}{R_o^2}$$

$$\frac{dr}{dx} = \cos\phi\,, \quad \frac{U}{r}\frac{dU}{dx}\frac{dr}{dx} = \frac{9U_\infty^2\sin^2\phi}{4R_o^2}$$

$$\frac{d^2r}{dx^2} = -\frac{\sin\phi}{R_o}\,, \quad \frac{U^2}{r}\frac{d^2r}{dx^2} = -\frac{9U_\infty^2\sin^2\phi}{4R_o^2}$$

The first term in Eq. 27 is

$$\frac{\mu U}{2\sqrt{\nu t}}\,\zeta_o''(0) = 3\mu\,\zeta_o''(0)\,\frac{U_\infty\sin\theta}{\sqrt{\nu t}}\,, \quad \zeta_o''(0) = 1.128$$

The second term is

$$\frac{\mu Ut}{2\sqrt{\nu t}}\left[\frac{dU}{dx}\,\zeta_{1a}''(0) + \frac{U}{r}\frac{dr}{dx}\,\zeta_{1b}''(0)\right]$$

$$= 9\frac{\mu t}{8\sqrt{\nu t}}\left[\zeta_{1a}''(0) + \zeta_{1b}''(0)\right]\frac{U_\infty^2}{R_o}\sin\phi\cos\phi$$

$$\zeta_{1a}''(0) = 1.614$$

$$\zeta_{1b}''(0) = 0.169$$

The third term of the series is

$$\frac{\mu Ut^2}{2\sqrt{\nu t}}\left[\left(\frac{dU}{dx}\right)^2\zeta_{2a}''(0) + \frac{Ud^2U}{dx^2}\,\zeta_{2b}''(0)\right.$$

$$+\frac{U}{r}\frac{dU}{dx}\frac{dr}{dx}\zeta_{2c}''(0) + \frac{U^2}{r}\frac{d^2r}{dx^2}\zeta_{2d}''(0) + \frac{U^2}{r^2}\left(\frac{dr}{dx}\right)^2\zeta_{2e}''(0)\Bigg]$$

$$= \frac{27\mu U_\infty{}^3 t^2}{16R_o{}^2\sqrt{\nu t}}\Bigg[+\zeta_{2a}''(0)\sin\theta\cos^2\theta + \zeta_{2b}''(0)\sin^3\theta$$

$$-\zeta_{2c}''(0)\sin\theta\cos^2\theta + \zeta_{2d}''(0)\sin^3\theta + \zeta_{2e}''(0)\sin\theta\cos^2\theta\Bigg]$$

$$\zeta_{2a}''(0) = -0.248$$

$$\zeta_{2b}''(0) = -0.068$$

$$\zeta_{2c}''(0) = -0.029$$

$$\zeta_{2d}''(0) = -0.022$$

$$\zeta_{2e}''(0) = 0.036$$

Substituting the above numerical values reduces the third term to

$$\sigma_{xy} = \frac{27\mu U_\infty{}^3 t^2}{16\sqrt{\nu t}R_o{}^2}\left[0.068\sin\theta - 0.309\sin\theta\cos^2\theta\right]$$

The total wall shear drag acting to decelerate the sphere is

$$D = \int_0^\pi \sigma_{xy} R_o{}^2 \sin^2\theta\, d\theta$$

The contribution to this by the first term is

$$D^{(1)} = \frac{3\mu\zeta_o''(0)U_\infty R_o^2}{\sqrt{\nu t}} \int_0^\pi \sin^3\theta \, d\theta$$

$$\int_0^\pi \sin^3\theta \, d\theta = -\frac{1}{3}\cos\theta\,(\sin^2\theta + 2) = \frac{4}{3}$$

The contribution to the wall shear drag by the second term is

$$D^{(2)} = \frac{9\mu t}{8\sqrt{\nu t}}\left[\zeta_{1a}''(0) + \zeta_{1b}''(0)\right] U_\infty^2 R_o \int_0^\pi \sin^3\theta\cos\phi \, d\theta$$

$$\int_0^\pi \sin^3\theta\cos\theta \, d\theta = \left[\frac{\sin^4\theta}{4}\right]_0^\pi = 0$$

Thus it can be seen that the second term makes no contribution to the total wall shear drag.

The contribution to the wall shear drag by the third term of the series is

$$D^{(3)} = \frac{27\mu U_\infty^3 t^2}{16\sqrt{\nu t}}\left[0.068\int_0^\pi \sin^3\theta \, d\theta - 0.309\int_0^\pi \sin^3\theta\cos^2\theta \, d\theta\right]$$

$$\int_0^\pi \sin^3\theta\sin^2\theta \, d\theta = \left[\frac{\cos\theta\sin^4\theta}{5}\right]_0^\pi + \frac{1}{5}\int_0^\pi \sin^3\theta \, d\theta$$

Then

$$D^{(3)} = \frac{27\mu U_\infty{}^3 t^2}{16\sqrt{\nu t}} \left[\frac{4}{3} \left(0.068 - \frac{0.309}{5}\right) \right]$$

Comparing the drags due to the first and third terms gives

$$\frac{D^{(3)}}{D^{(1)}} = 0.0031 \left[\frac{U_\infty t}{R_o}\right]^2$$

The largest value of this ratio during the propulsive force pulse occurs at the end of the pulse where

$$U_\infty = 51.71 \text{ in. sec.}^{-1}$$

$$t = 4.028 \text{ sec.}$$

$$R_o = 0.502$$

giving

$$\left[\frac{U_\infty t}{R_o}\right] = 0.415, \quad \left[\frac{U_\infty t}{R_o}\right]^2 = 0.172$$

at this time

$$\frac{D^{(3)}}{D^{(1)}} = 0.00053$$

Thus

$$D^{(3)} \leq 0.00053\, D^{(1)} \quad \text{for} \quad 0 \leq t \leq \frac{T}{2}$$

where $\frac{T}{2}$ is the duration of the force pulse.

Then

$$\int_0^{T/2} D^{(3)}dt \leqq 0.00053 \int_0^{T/2} D^{(1)}dt$$

Hence the wall shear impulse due to the third term of the shear stress series is negligible in comparison to that due to the first term of the series.

Since the series for the shear stress is in powers of

$$\frac{U_\infty t}{R_o}$$

the higher order terms decrease in magnitude. Hence the viscous wall shear drag and the impulse due to it during the propulsive force interval are given with very good accuracy by considering only the first term of Eq. 27, corresponding to the solution for flow over a flat plate.

APPENDIX 2

The Free Stream Velocity for Flow About a Sphere on the Axis of a Circular Cylinder

The velocity of the fluid at the surface of the sphere can be found from the vector potential determined by W. R. Smythe in his paper entitled "Flow Around a Spheroid in a Circular Tube". (3)

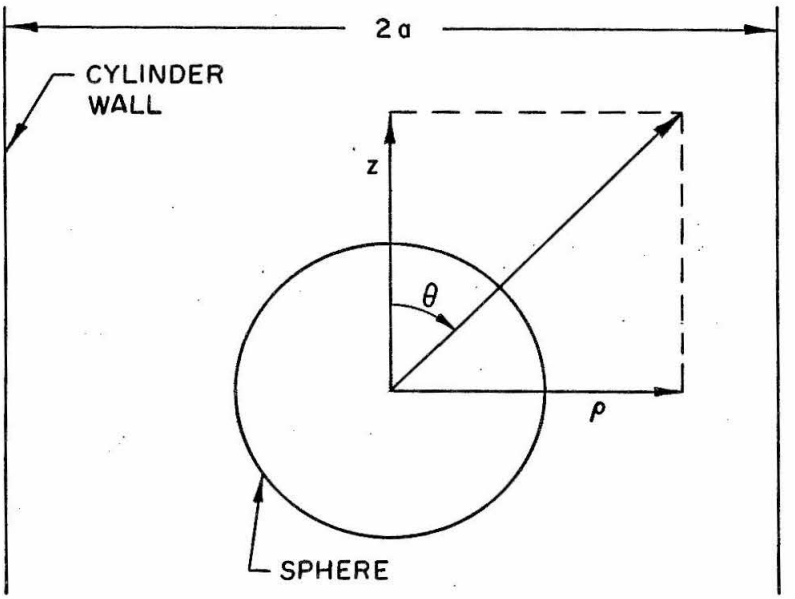

Fig. 2A - Co-ordinates

In this paper the vector potential is given by

$$A_\phi = A_\phi^{o} + A_\phi^{''} + A'^{''}_\phi \tag{17}$$

where

$$A_\phi^{o} = \frac{1}{2} v_o \rho \tag{2}$$

$$A_\phi^{''} = v_o \sum_{n=0}^{N} \frac{v_o \rho_o C_n}{(4n+3)} \left(\frac{c}{r}\right)^{2n+2} P^1_{2n+1}(\xi) \tag{5}$$

$$A'^{''}_\phi = v_o \sum_{\rho=0}^{N} A_p \left(\frac{r}{a}\right)^{2p+1} P^1_{2p+1}(\xi) \tag{11}$$

$$A_p = \frac{c(-1)^{n+p+1} \left(\frac{c}{a}\right)^{2n+2} I(2n+2p+2) C_n}{\pi (2n)! \left(2n+\frac{3}{2}\right)(2n+2p+3)(2p+2)!} \tag{12}$$

Here the number in parentheses at the end of each equation is the equation number in Smythe's paper.

v_o is the flow velocity far from the sphere, which is equivalent to the velocity of the sphere in the cylinder, U_∞, in the viscous flow problem solved in Section IV.

c is defined in Smythe's paper as the radius of the sphere, i.e., $c = \rho_o$.

The orientation of the spherical polar co-ordinate system (r, θ, ϕ) is shown in Fig. 2A where the radii ρ and a are also shown.

C_n are constant coefficients

$P^1_{(2n+1)}$ are associated Legendre polynomials

I is an integral which is defined and evaluated in Table 1 of Reference 3.

The velocity at any point is

$$V = \text{curl } A_\phi \tag{18}$$

The velocity at the surface of the sphere is given by

$$\text{Curl}_\theta A_\phi = \frac{1}{r} \frac{\partial(-rA_\phi)}{\partial r}$$

Now

$$\text{Curl}_\theta A^o_\phi = \frac{1}{r} \frac{\partial(\frac{1}{2} v_o r^2 \sin\theta)}{\partial r} = + v_o \sin\theta$$

$$\text{Curl}_\theta A_\phi'' = \sum_{n=0}^{N} \frac{v_o \rho_o C_n (2n+1)}{(4n+3)r} \left(\frac{c}{r}\right)^{2n+2} P^1_{2n+1}(\xi)$$

$$\text{Curl}_\theta A'^{''}_\phi = - v_o \sum_{p=0}^{N} \frac{A_p (2p+2)}{r} \left(\frac{r}{a}\right)^{2p+1} P^1_{2p+1}(\xi)$$

For n = 0 :

$$\text{Curl}_\theta A_\phi'' = \frac{v_o \rho C_o P_1^1(\xi)}{3c}$$

$$P_1^1 = (1 - \xi^2)^{\frac{1}{2}} = (1 - \cos^2\theta)^{\frac{1}{2}} = \sin\theta \tag{10}$$

$$\text{Curl}_\theta A_\phi'' = \frac{v_o \rho C_o \sin\theta}{3c} = \frac{C_o v_o \sin\theta}{3}$$

For n = 0:

$$A_p = \frac{c(-1)^{p+1}\left(\frac{c}{a}\right)^2 I(2p+2) C_o}{\pi\left(\frac{3}{2}\right)(2p+3)(2p+2)!}$$

p = 0:

$$A_o = \frac{-c\left(\frac{c}{a}\right)^2 I(2) C_o}{9\pi}$$

$$\text{Curl}_\theta A_\phi'' = \frac{2}{9\pi}\left(\frac{c}{a}\right)^3 I(2) C_o v_o \sin\theta$$

p = 1:

$$A_1 = \frac{c\left(\frac{c}{a}\right)^2 I(4) C_o}{180\pi}$$

$$\text{Curl}_\theta A_\phi'' = \frac{-\left(\frac{c}{a}\right)^2 I(4) C_o}{45\pi}\left(\frac{c}{a}\right)^3 v_o P^1{}_3(\xi)$$

$$P^1{}_3(\xi) = \frac{3}{2}\sin\theta(5\cos^2\theta - 1) \qquad (10)$$

$$\text{Curl}_\theta A_\phi'' = \frac{1}{30\pi}\left(\frac{c}{a}\right)^5 I(4) C_o v_o \sin\theta\,(1 - 5\cos^2\theta)$$

p = 2:

$$\text{Curl } A'''_{\phi} = \frac{6\, I(6)}{\pi(\frac{3}{2})(7)(6!)} \left(\frac{c}{a}\right)^7 C_o v_o P^1_5$$

Table 1 of Ref. 3 gives

$$I(2) = 7.5099$$

$$I(4) = 4 \times 4.7142 .$$

Using only the terms for n = 0 and p = 0 and 1, the velocity at the surface of the sphere where $c = r = R_o$ is given by

$$U(\theta) = U_\infty \sin\theta \left[1 + \frac{C_o}{3} + 0.5312 \left(\frac{R_o}{a}\right)^3 C_o + 0.2001 \left(\frac{R_o}{a}\right)^5 C_o \right.$$

$$\left. - 1.000 \left(\frac{R_o}{a}\right)^5 C_o \cos^2\theta + \ldots . \right] \qquad \text{(Eq. 39)}$$

The error in neglecting terms where $n > 0$ depends upon the ratio R_o/a. The error increases as the ratio of the sphere to cylinder diameter decreases. For the largest cylinder used, $R_o/a = 0.226$. The error in neglecting terms for $n > 0$ is less than the error for $R_o/a = 0.3$, for which, from Table 3 of Ref. 7, $C_o = 1.53298$ and $C_1 = -0.000870$, and successive C_n are decreasing rapidly. Thus $C_1/C_o = 0.0005$ which indicates the order of magnitude of the n = 1 term compared with the n = 0 term. Thus great accuracy is achieved for the largest cylinder, the one in which the tests in oil were conducted, by using only the n = 0 term. The values of C_1/C_o are shown for various R_o/a in Table 1A.

The error in neglecting terms for $p > 1$ also depends upon the ratio R_o/a. The term $A'_{\phi}{}''$ of the vector potential is an expansion involving $(\frac{R_o}{a})^{2p+3}$. Thus the ratio of successive terms in R_o/a is $(\frac{R_o}{a})^2$. For the cylinder in which the tests in oil were conducted,

$$\frac{R_o}{a} = 0.226 \quad \text{and} \quad (\frac{R_a}{a})^2 = 0.0511$$

and keeping terms up to and including the powers of $(\frac{R_o}{a})^5$ leaves an error in the magnitude of $U(\theta)$ on the order of $(\frac{R_o}{a})^7 \approx 0.00003$. The value of $(\frac{R_o}{a})^7$ for the various test cylinders is shown in Table 1A.

Table 1A

$\frac{R_o}{a}$ Versus $(\frac{R_o}{a})^7$ and $\frac{C_1}{C_o}$

$\frac{R_o}{a}$	$(\frac{R_o}{a})^7$	$\frac{R_o}{a}$	$\frac{C_1}{C_o}$
0.226	0.00003	0.2	-0.00010
0.289	0.0002	0.3	-0.00087
0.409	0.0019	0.4	-0.00141
0.518	0.010	0.5	-0.00731
0.585	0.023	0.6	-0.0183
0.680	0.067	0.7	-0.0403
0.812	0.233*	0.8	-0.0823
0.905	0.50	0.9	-0.168

* For $\frac{R_o}{a} = 0.812$ the exact value of the term for $C = 0$ and $p = 2$ is given from Smythe's equation 11 as follows:

$$\text{Curl } A'_{\phi}{}'' = \frac{6\, I(6)}{\pi(\frac{3}{2})(7)(6!)} (\frac{R_o}{a})^7 C_o U_\infty P_5'$$

From Table 1, Ref. 3

$$(3!)^{-2} I(6) = 4.556$$

Then

$$I(6) = 164.0$$

For $\left(\frac{R_o}{a}\right) = 0.812$, $\left(\frac{R_o}{a}\right)^7 = 0.233$, $C_o = 2.7177$

$$P_5^1(\xi) = (1 - \xi^2)^{\frac{1}{2}} \frac{dP_5 \xi}{d\xi}$$

$$P_5(\xi) = \frac{1}{8} (63\xi^5 - 70\xi^3 + 15\xi)$$

$$P_5'(\xi) = \frac{\sin\theta}{8} (315 \cos^4\theta - 210 \cos^2\theta + 15)$$

So for n = 0, p = 2

$$\text{Curl } A_\phi'' = C_o U_\infty \sin\theta (0.0181 - 0.253 \cos^2\theta + 0.394 \cos^4\theta)$$

The contribution of this term to the integral $\int_0^\pi U(\theta)\sin^2\theta \, d\theta$

in Eq. 42 follows.

The required integrals are

$$\int_0^\pi \sin^3\theta \, d\theta = \frac{4}{3}; \quad \int_0^\pi \cos^2\theta \sin^3\theta \, d\theta = \frac{4}{15}$$

$$\int_0^{\pi} \cos^4\theta \sin^3\theta \, d\theta = \frac{4}{35}$$

Then the contribution to

$$\int_0^{\pi} U(\theta) \sin^2\theta \, d\theta$$

is $0.0046\ U_\infty$. Expressed as a percentage of the sum of the terms for p = 0 and p = 1, this is

$$\frac{0.0046}{3.475} \times 100\% = 0.1327\%$$

giving the percentage error of the first neglected term. The error in I_D/M in Table 12 is then

$$0.6153 \times \frac{0.1327}{100} = 0.0008 \text{ in. sec.}^{-1}$$

APPENDIX 3

Evaluation of the Shear Drag and the Impulse Due to This Drag During the Force Pulse Period

The impulse due to the wall shear drag is given by

$$I_D = \frac{2\rho\sqrt{\frac{\nu}{\pi}} \int_0^{\pi} 2\pi R_o^2 \sin^2\theta \, U(\theta) \, d\theta \int_0^{T/2} \sqrt{\frac{T}{2} - \tau} \; e^{-2a\tau} \sin^2 \omega\tau \, d\tau}{\int_0^{T/2} e^{-2a\tau} \sin^2 \omega\tau \, d\tau}$$

(Eq. 42)

Let

$$\int_0^{T/2} e^{-2a\tau} \sin^2 \omega\tau \, d\tau = I_1$$

$$I_1 = \frac{\omega}{4(\omega^2 + a^2)} \left[\frac{\omega}{a}\left(1 - e^{-aT}\right)\right]$$

Using the values of a, ω and T from Section IV.B

$$I_1 = 0.9670 \times 10^{-3} \text{ sec.}$$

Let

$$\int_0^{T/2} \sqrt{\frac{T}{2} - \tau}\ e^{-2a\tau} \sin^2 \omega\tau\, d\tau = I_2$$

This integral was evaluated numerically by Simpson's rule using the following table of numerical values.

Table 2A

Table of Values for I_2

τ	$e^{-2a\tau}$	$\sin^2\omega\tau$	$\sqrt{\frac{T}{2} - \tau}$	$\sqrt{\frac{T}{2} - \tau}\, e^{-2a\tau}\sin^2\omega\tau$	For Simpson's Rule
0×10^{-3}	1	0	6.347×10^{-2}	0×10^{-2}	$y_0 = 0 \times 10^{-2}$
0.504	0.8220	0.1465	5.936	0.7148	$4y_1 = 2.8592$
1.007	0.6760	0.5000	5.496	1.8576	$2y_2 = 3.7152$
1.511	0.5528	0.8536	5.018	2.0212	$4y_3 = 8.0848$
2.014	0.4571	1	4.488	2.0515	$2y_4 = 4.1030$
2.519	0.3759	0.8536	3.885	1.2584	$4y_5 = 5.0336$
3.021	0.3088	0.5000	3.174	0.4901	$2y_6 = 0.9801$
3.525	0.2539	0.1465	2.243	0.0834	$4y_7 = 0.3336$
4.028	0.2092	0	0	0	$y_8 = 0$
					$\sum = 25.1095$

$$I_2 = \frac{h}{3}\sum a_n y_n = \left(\frac{4.028 \times 10^{-3}}{24}\right)(25.11 \times 10^{-2})\,\text{sec.}^{\frac{3}{2}}$$

$$= 4.214 \times 10^{-5}\,\text{sec.}^{\frac{3}{2}}$$

Let

$$\int_0^{\pi} \sin^2\theta\, U(\theta)\, d\theta = I_3$$

$$U(\theta) = U_\infty \sin\theta \left[1 + \frac{C_o}{3} + 0.5312 \left(\frac{R_o}{a}\right)^3 C_o + 0.2001 \left(\frac{R_o}{a}\right)^5 C_o \right.$$

$$\left. + 1.000 \left(\frac{R_a}{a}\right)^5 C_o \cos^2\theta \right] \qquad \text{(Eq. 39)}$$

The derivative of this equation is shown in Appendix 1.

For the cylinder used in the tests

$$C_o = 1.5157, \quad \frac{R_o}{a} = 0.226 \qquad \text{and}$$

$$U(\theta) = U_\infty(1.5147 \sin\theta - 0.0009 \cos^2\theta \sin\theta)$$

Then

$$I_3 = \frac{4}{3}\,(1.5145)$$

Equation 42 can now be written

$$I_D = \frac{4\rho R_o^2 \sqrt{\pi\nu}\, I_3 I_2}{I_1} U_\infty \left(\frac{T}{2}\right)$$

Using the measured values

$$\rho = 0.8806 \pm 0.0002 \text{ gm.cm.}^{-3}$$

$$\nu = 63.61 \pm 0.20 \text{ centipoises}$$

$$U_\infty = 51.79 \pm 0.07 \text{ in.sec.}^{-2}$$

$$R_o = 0.5020 \pm 0.0001 \text{ in.}$$

the result is

$$I_D = 38.94 \pm 0.07 \text{ gm.in.sec.}^{-1} .$$

The error in the integrals I_1, I_2 and I_3 due to the experimental error in the evaluation of the constants α and ω are very small and hence are assumed negligible here.

The drag D at time T/2 when the force pulse was over is given by

$$D = \frac{\rho \sqrt{\frac{\nu}{\pi}} \int_0^{\pi} 2\pi R_o^2 \sin^2\theta \, U(\theta) \, d\theta \int_0^{T/2} \frac{e^{-2\alpha\tau} \sin^2 \omega\tau \, d\tau}{\sqrt{(t - \tau)}}}{\int_0^{T/2} e^{-2\alpha\tau} \sin^2 \omega\tau \, d\tau} \qquad \text{(Eq. 41)}$$

Let

$$\int_0^{T/2} \frac{e^{-2\alpha\tau} \sin^2 \omega\tau \, d\tau}{\sqrt{(t - \tau)}} = I_4$$

I_4 was evaluated by using Simpson's rule in the same way as I_2 using the following table of numerical values.

Table 3A

Table of Values for I_3

τ	$\sqrt{\frac{T}{2} - \tau}$	$e^{-2a\tau}\sin^2\omega\tau$	$\frac{e^{-2a\tau}\sin^2\omega\tau}{\sqrt{\frac{T}{2} - \tau}}$	For Simpson's Rule
0×10^{-3}	6.347×10^{-2}	0	0×10^{-2}	$y_0 = 0 \times 10^{-2}$
0.504	5.936	0.1204	0.02028	$4y_1 = 0.08112$
1.007	5.496	0.3380	0.06150	$2y_2 = 0.12300$
1.511	5.018	0.4719	0.09404	$4y_3 = 0.37616$
2.014	4.488	0.4571	0.10185	$2y_4 = 0.20370$
2.519	3.885	0.3209	0.08260	$4y_5 = 0.33040$
3.021	3.174	0.1544	0.04865	$2y_6 = 0.09730$
3.525	2.243	0.0372	0.01658	$4y_7 = 0.06632$
4.028	0	0	0	0

$$\sum = 1.2780 \times 10^{-2}$$

$$I_4 = \frac{h}{3}\sum a_n y_n = \left(\frac{4.028 \times 10^{-3}}{24}\right)(1.2780 \times 10^{2})\,\text{sec.}^{\frac{1}{2}}$$

$$= 2.1449 \times 10^{-2}\,\text{sec.}^{\frac{1}{2}}$$

Equation 41 then reduces to

$$D = \frac{2\rho R_o^{2}\sqrt{\pi\nu}\; I_3 I_4 U_\infty \left(\frac{T}{2}\right)}{I_1}$$

Substituting the measured values of ρ, R_o, ν and U_∞ into this equation gives

$$D = 0.991 \pm 0.002\ \text{gm.in.sec.}^{-2}$$

Here the units as well as the units in I_D are mixed for convenience in calculation.

APPENDIX 4

Figures

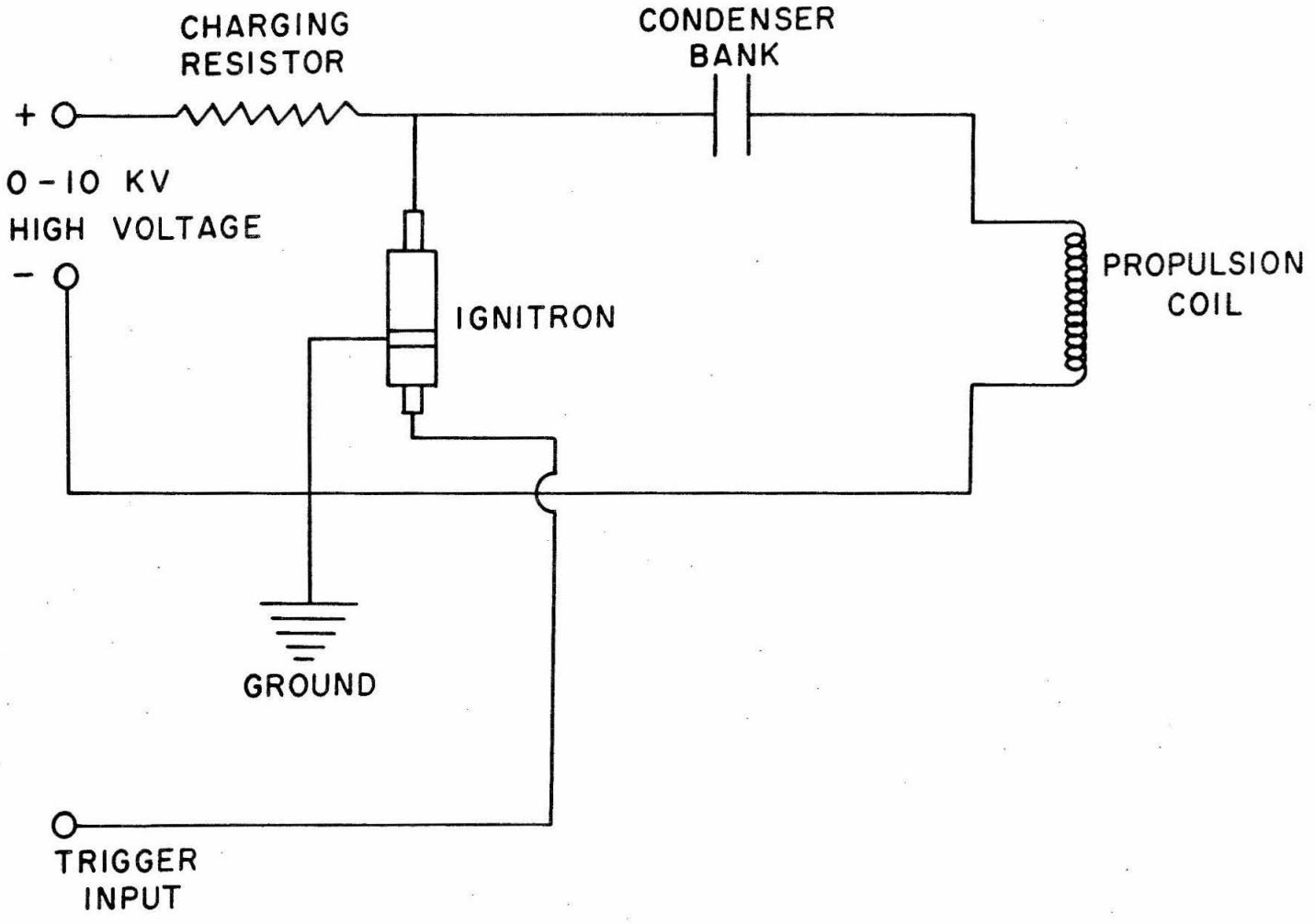

Fig. 3A - The electromagnetic propulsion system

Fig. 4A - Lucite water tank with camera and highlight source. The propulsion coil and its mount are shown together with the sphere in its initial position.

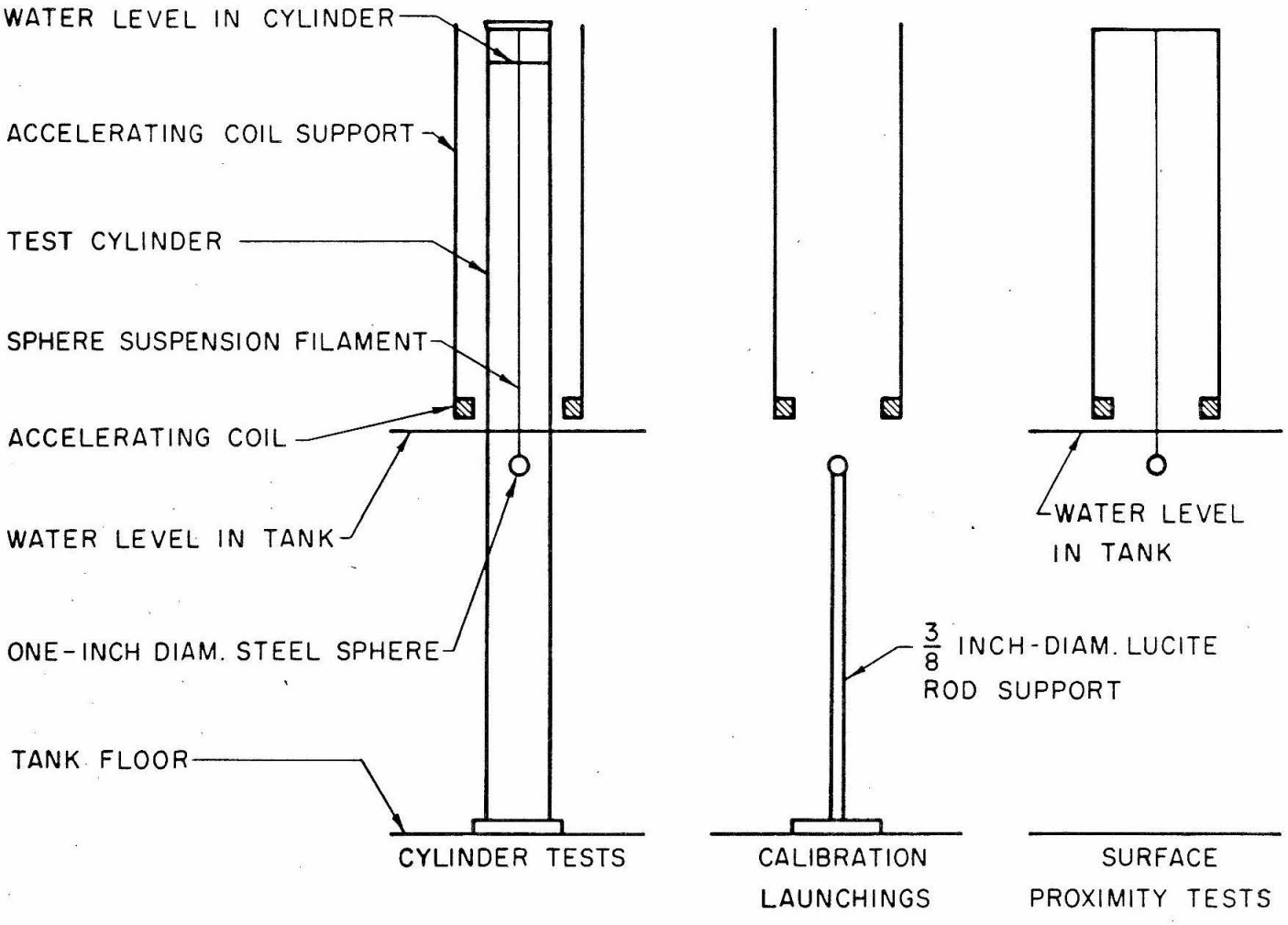

Fig. 5A - The various methods used for placing the test sphere in its initial position

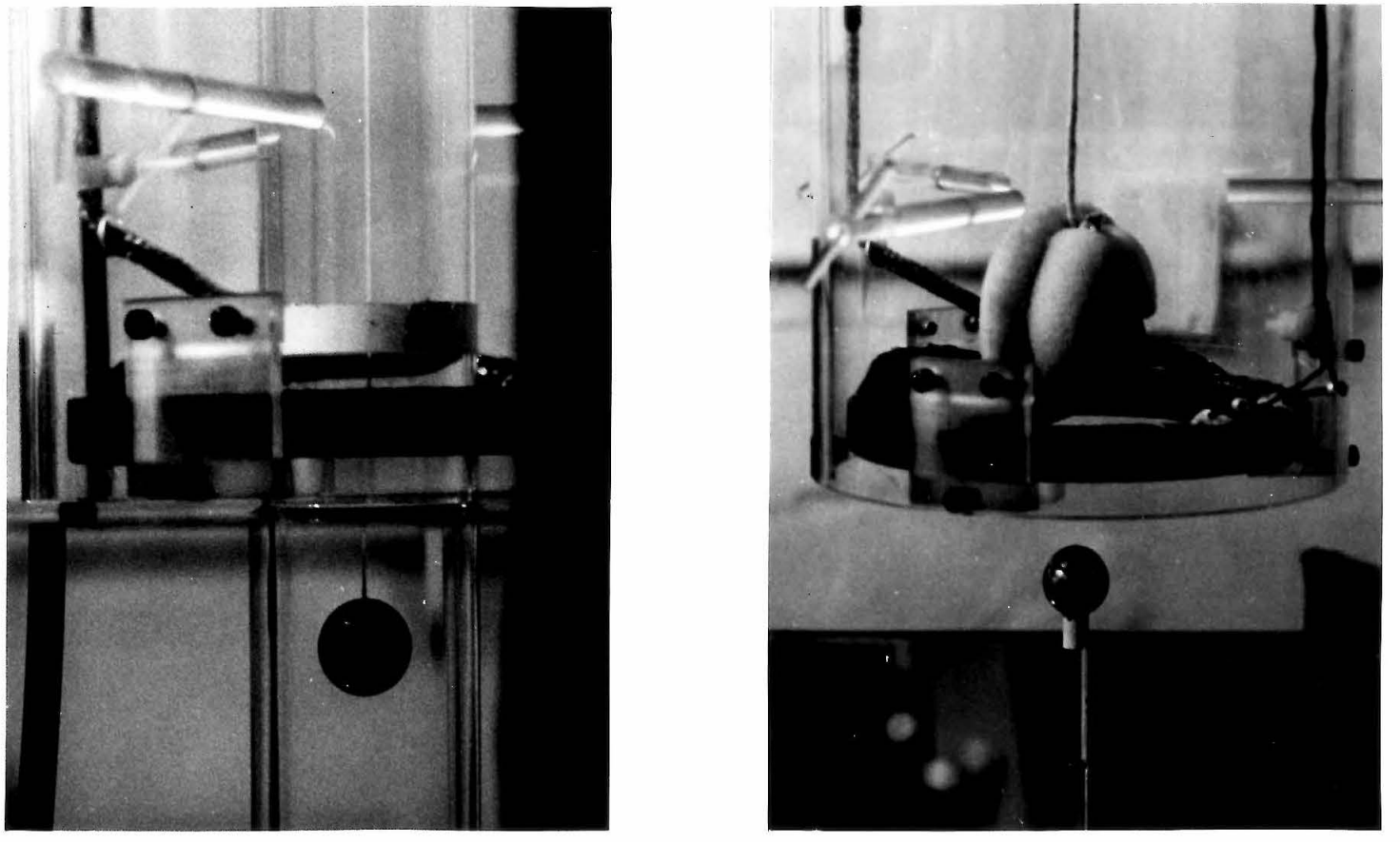

Fig. 6A - Sphere located in its initial position beneath propulsion coil ready for test.

Left - Sphere suspended by thread in water in a test cylinder.

Right - Sphere in air resting on lucite rod.

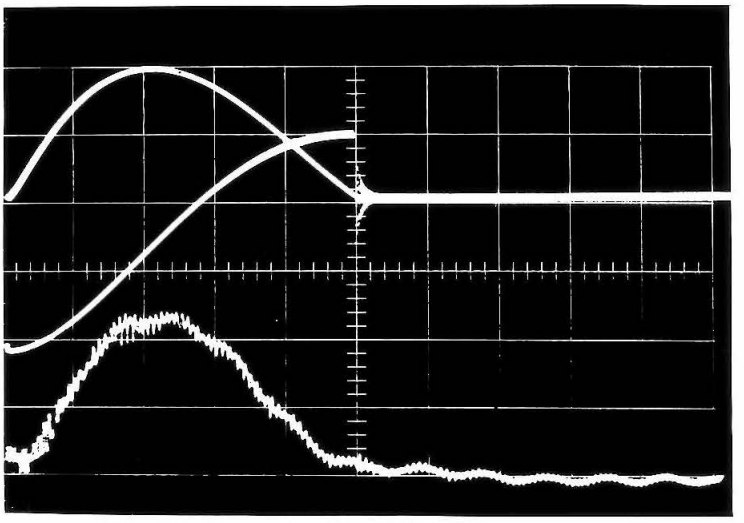

Fig. 7A -

Top

Oscilloscope trace of propulsion coil voltage and current versus time.

Bottom

Oscilloscope trace of electro-magnetic force of propulsion coil on test sphere versus time.

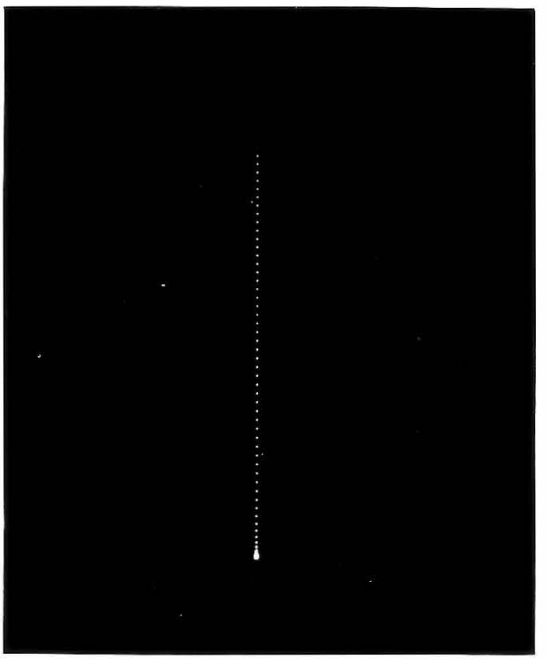

Fig. 8A - Highlight film of 1-inch-diameter sphere moving vertically upward in water. Time between successive exposures 1/1000 second.

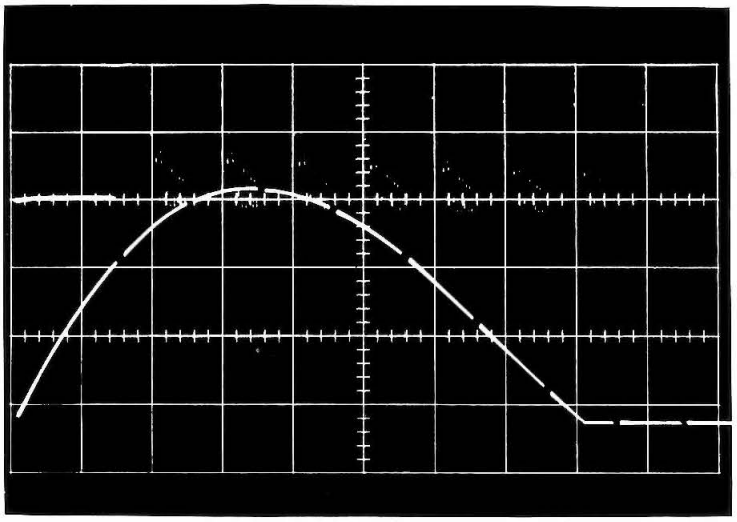

Fig. 9A - Oscilloscope trace of current in propulsion coil interrupted when highlight flashes occurred. Time interval between flashes 1/2000 second.

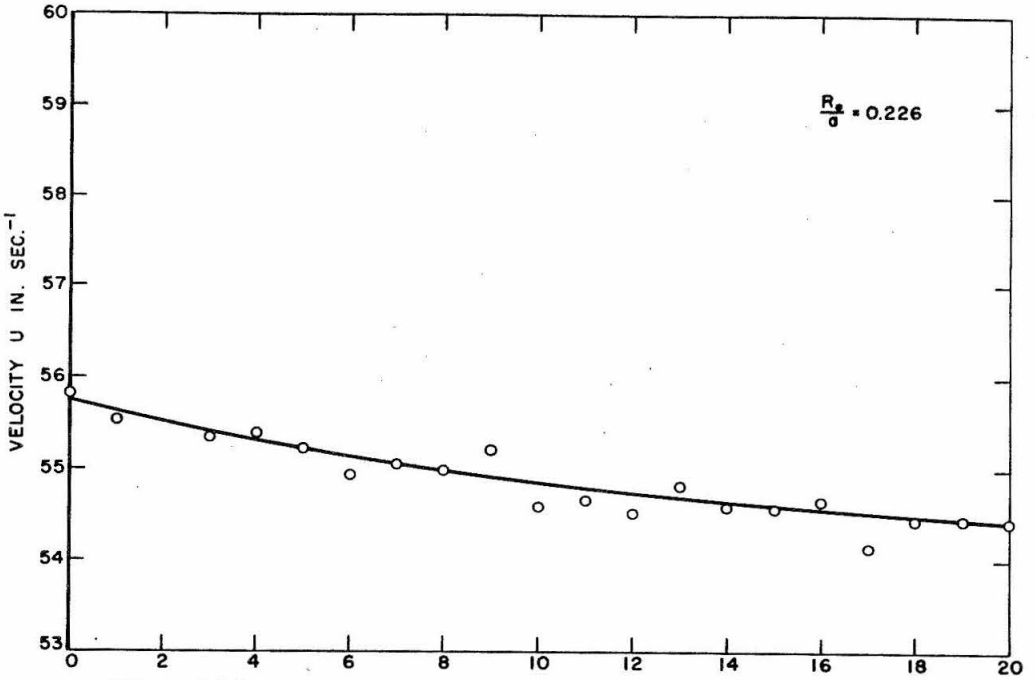

Fig. 10A

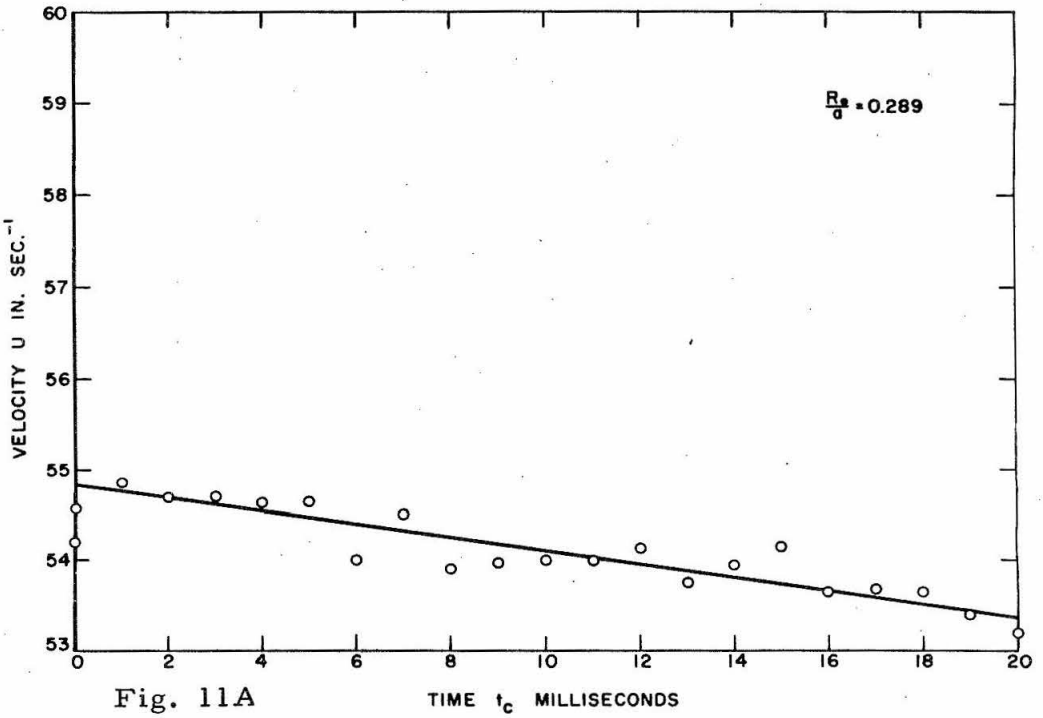

Fig. 11A

Figs. 10A and 11A - Vertical upward velocity of sphere in water along cylinder axis after propulsive force

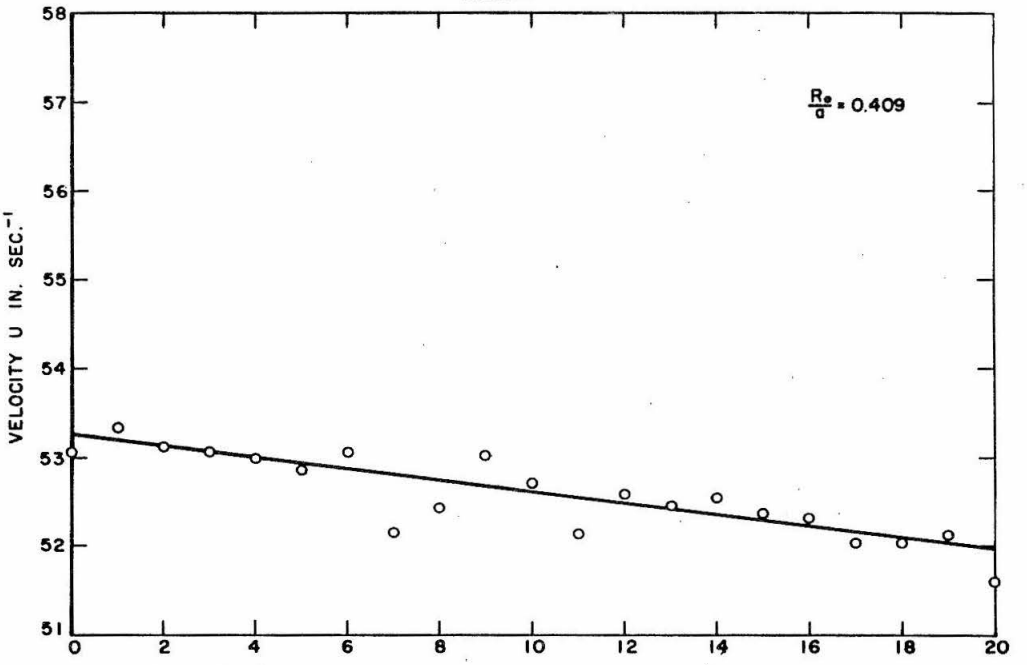

Fig. 12A

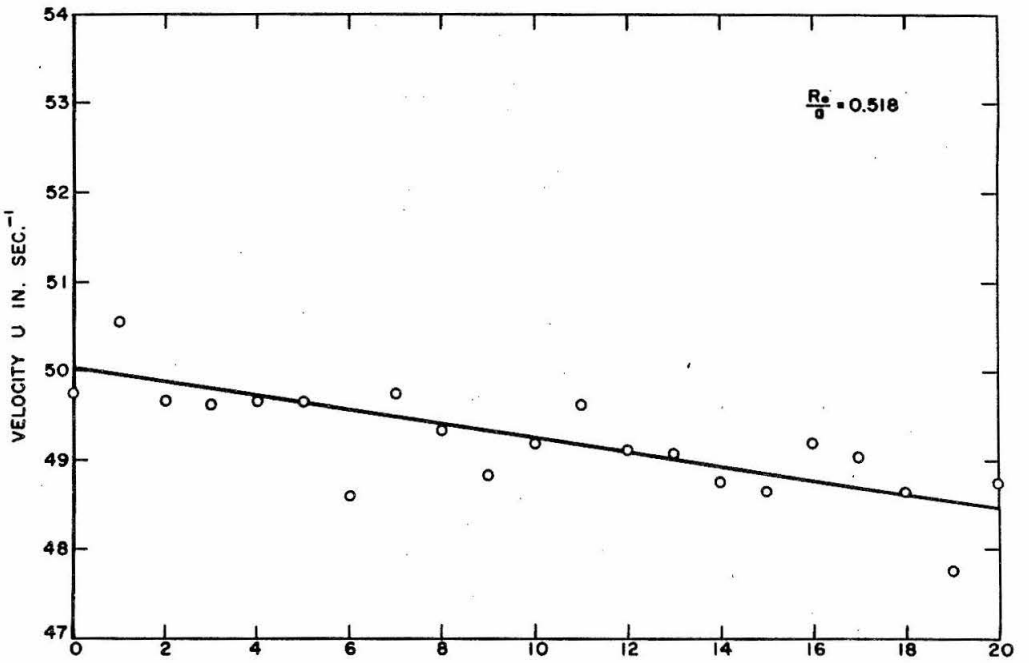

Fig. 13A

Figs. 12A and 13A - Vertical upward velocity of sphere in water along cylinder axis after propulsive force

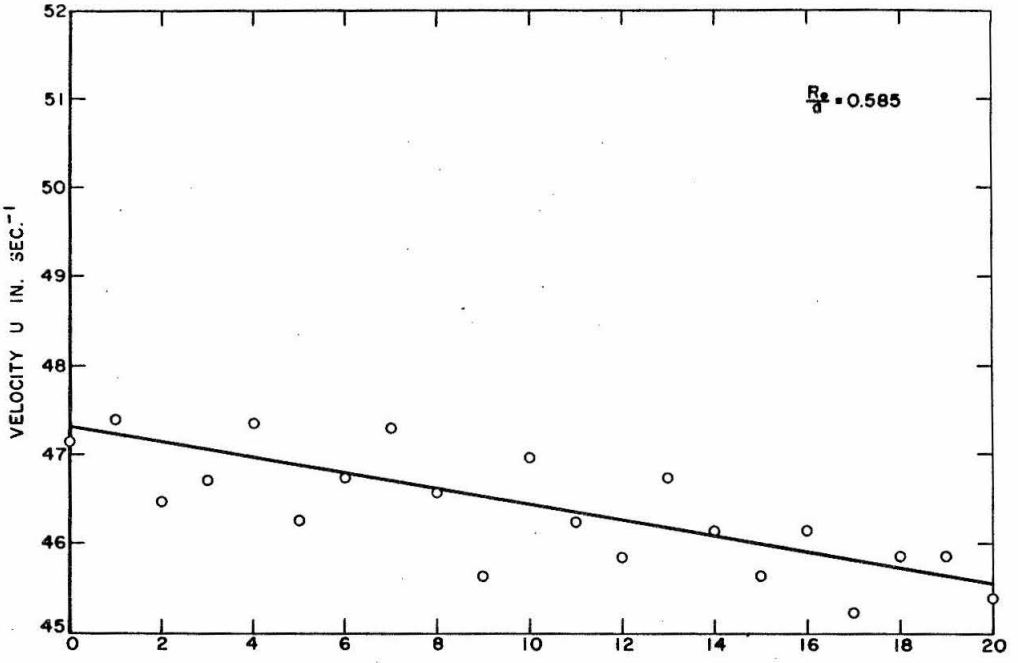

Fig. 14A

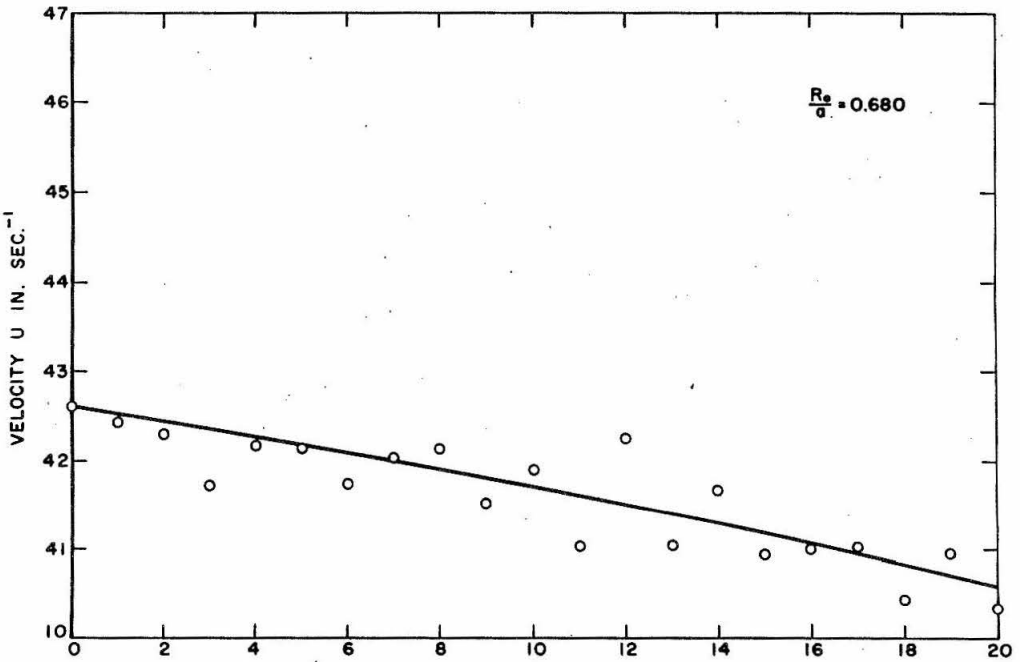

Fig. 15A

Figs. 14A and 15A - Vertical upward velocity of sphere in water along cylinder axis after propulsive force

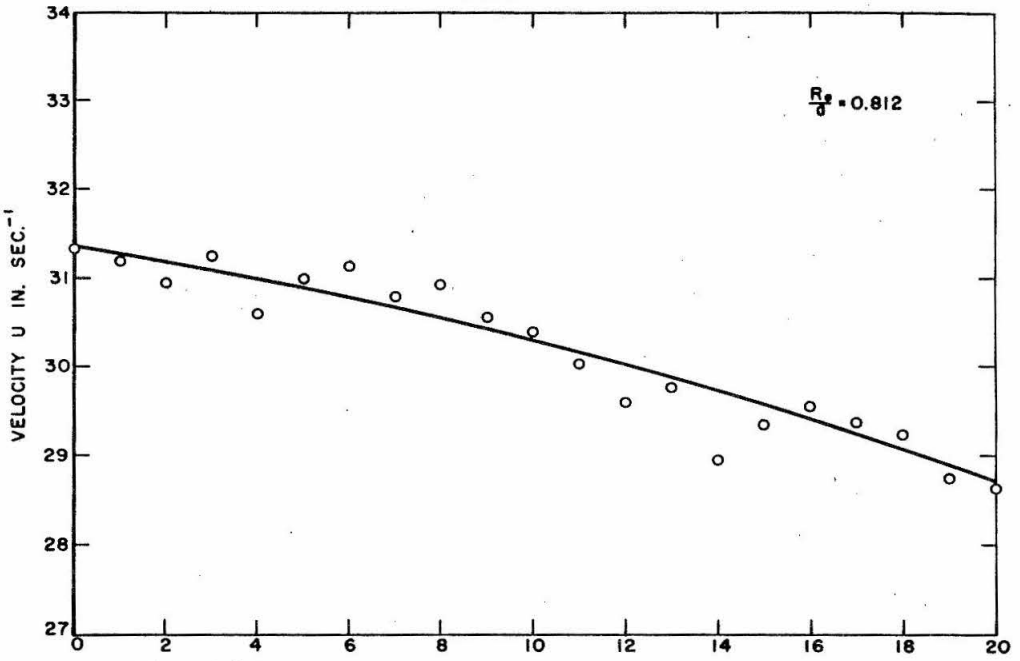

Fig. 16A

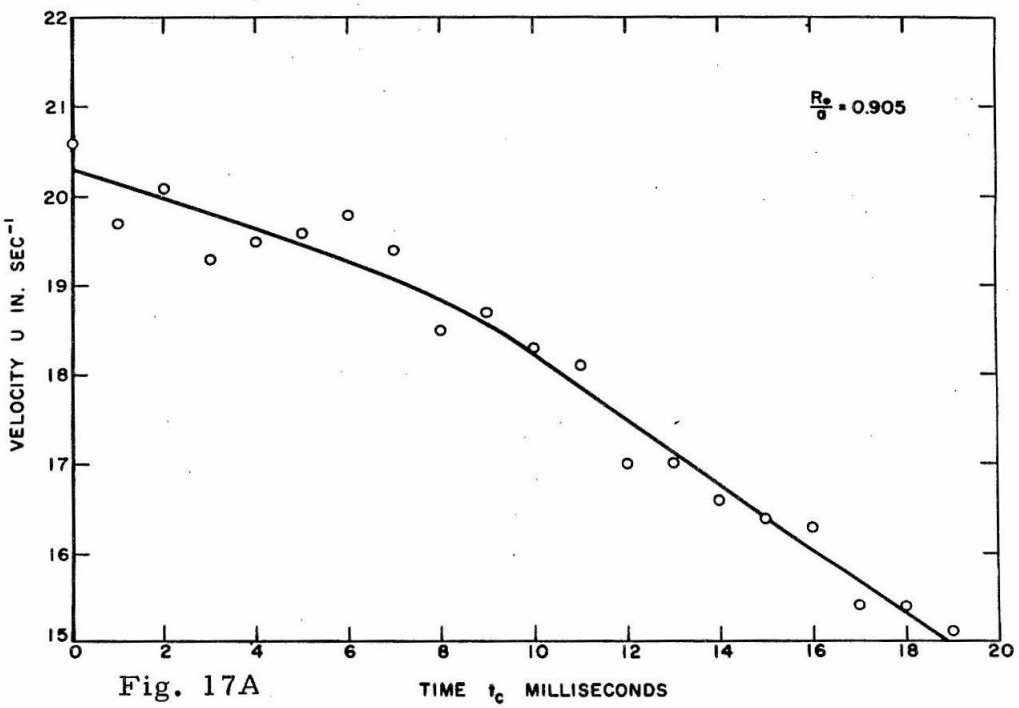

Fig. 17A

Figs. 16A and 17A - Vertical upward velocity of sphere in water along cylinder axis after propulsive force

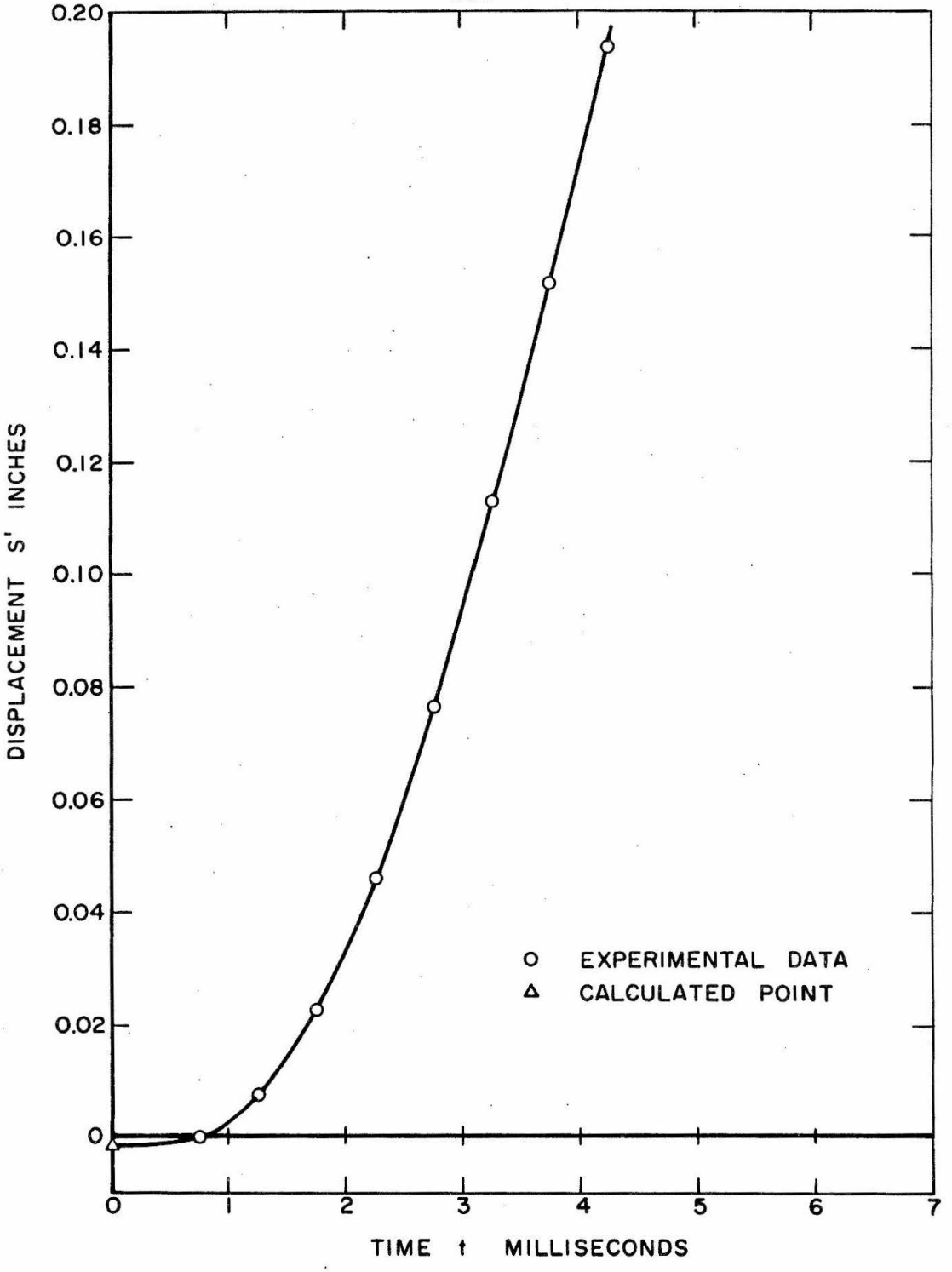

Fig. 18A - A vertical upward displacement of 1.004 inch diameter sphere in air versus time after start of propulsive force

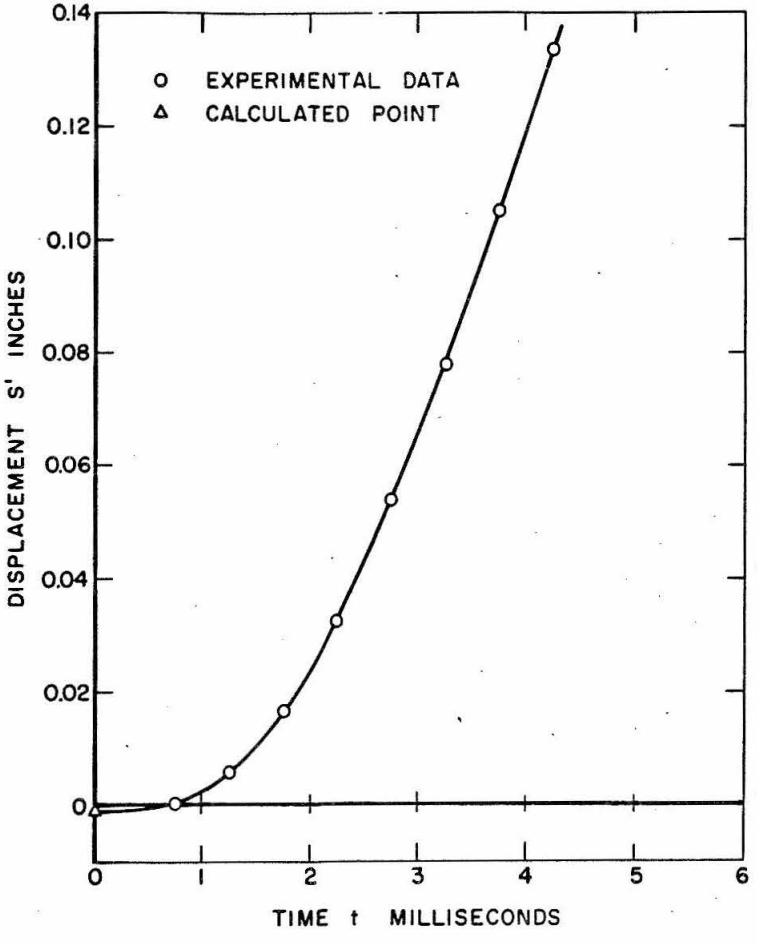

Fig. 19A - Sphere in water

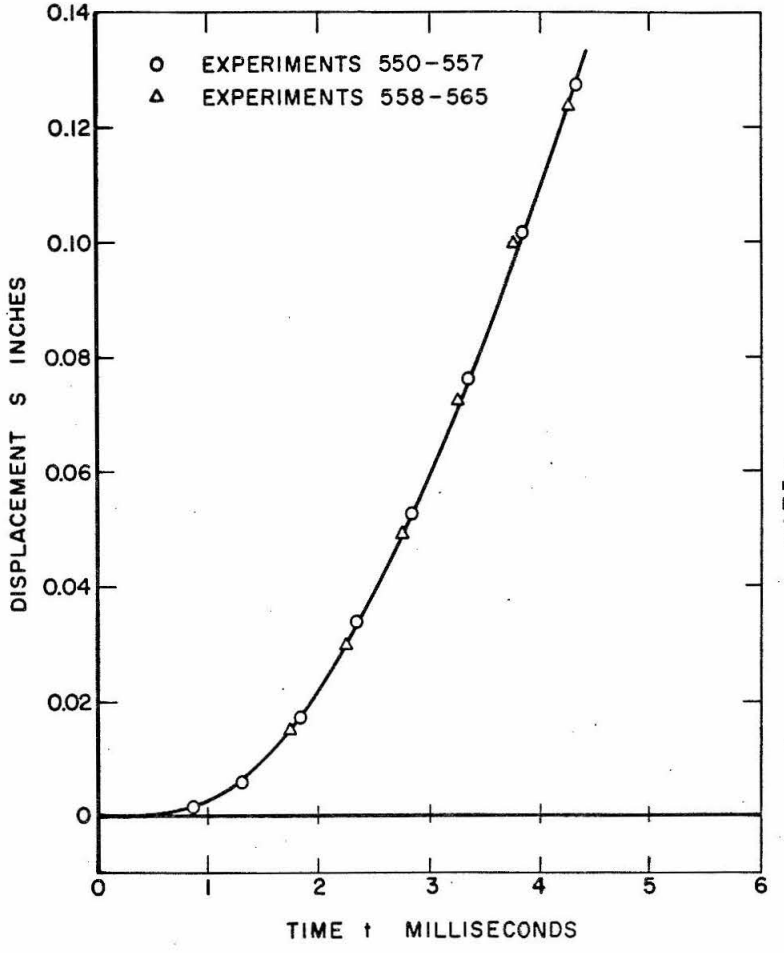

Fig. 20A - Sphere in No. 7 mineral oil

Figs. 19A and 20A - Vertical upward displacement of 1.004 inch diameter sphere along axis of 4.45 inch I.D. cylinder versus time after start of propulsive force

APPENDIX 5

Nomenclature

R_o	radius of sphere
a	radius of cylinder
C_o	constant coefficient depending upon $\frac{R_o}{a}$
m	added mass of sphere in fluid
ρ	density of fluid medium
A	cross sectional area of the circular cylinder
V	volume of fluid displaced by the sphere
F_w	axial magnetic force applied to the sphere in water
I_{F_w}	net propulsive impulse applied to the sphere in water
G_w	net gravitational force acting to accelerate the sphere in water
t	time
$\frac{T}{2}$	time duration of propulsive force pulse
M	mass of sphere
U_w	velocity of the sphere in water at the end of the propulsive force pulse
F_a	axial magnetic force applied to the sphere in air
I_{F_a}	net propulsive impulse applied to the sphere in air

G_a	gravitational force acting on the sphere in air
U_a	velocity of the sphere in air
I_{G_w}	net impulse on sphere in water due to gravity during the propulsive force period
z	distance from center of test sphere to center of propulsive coil
z_o	the value of z at the initial sphere position
a	damping constant of the propulsion coil - capacitor circuit
ω	natural frequency of the propulsion coil - capacitor circuit
g	gravitational acceleration
c	radius of propulsion coil
U_∞	velocity of sphere in oil at the end of the propulsive force pulse
b	slope of least square straight line of velocity time curve for specified time interval after force pulse was over
I	current in propulsion coil
$U(\theta)$	potential flow velocity at surface of the sphere
u	velocity of viscous fluid around the sphere
r	perpendicular horizontal distance from the axis of the sphere in boundary layer theory
μ	dynamic viscosity of the fluid
ν	kinematic viscosity of the fluid
$\zeta_{\alpha\beta}''(0)$	numerical coefficients of the series solution to the boundary layer equations evaluated by E. Boltze (8)

p	fluid pressure
σ_{xy}	skin friction at the sphere surface
Ω	fluid vorticity
A_ϕ	vector potential for flow around a sphere in a circular cylinder
F_o	magnetic propulsive force for sphere in oil
D	drag on sphere due to wall shear stress
I_D	impulse on sphere due to wall shear stress during the time of the propulsive force pulse
G_o	buoyancy force of sphere in oil
M_D	mass of fluid carried along in the boundary layer of the sphere due to shear force in the fluid
t_c	time elapsed after the propulsive force stopped